Bioprinting 21 (2021) e00116

Contents lists available at ScienceDirect

Bioprinting

journal homepage: www.elsevier.com/locate/bprint

Extrusion bioprinting: Recent progress, challenges, and future opportunities

Srikanthan Ramesh [a], Ola L.A. Harrysson [b], Prahalada K. Rao [c], Ali Tamayol [d], Denis R. Cormier [a], Yunbo Zhang [a], Iris V. Rivero [a,*]

[a] Department of Industrial and Systems Engineering, Rochester Institute of Technology, Rochester, 14623, USA
[b] Edward P. Fitts Department of Industrial and Systems Engineering, North Carolina State University, Raleigh, 27695, USA
[c] Department of Mechanical and Materials Engineering, University of Nebraska-Lincoln, Lincoln, 68588, USA
[d] Department of Biomedical Engineering, University of Connecticut Health Center, Farmington, 06030, USA

ARTICLE INFO

Keywords:
Extrusion-based bioprinting
Bioinks
Printability
Rheology
Tissue engineering
Scaffolds

ABSTRACT

Extrusion-based bioprinting involves extrusion of bioinks through nozzles to create three-dimensional structures. The bioink contains living organisms with biological relevance for emerging applications such as tissue scaffolds, organs-on-a-chip, regenerative medicine, and drug delivery systems. Bioinks, which are mixtures of biomaterials and living cells, influence the quality of printed constructs through their physical, mechanical, biological, and rheological behavior. Printability is a property of a bioink used to describe its ability to create well-defined structures. Amongst all contributing factors, rheological properties and printing parameters are primary factors that influence the quality of bioprinted constructs. With the increasing popularity of extrusion bioprinting, different approaches for controlling these properties and parameters have emerged. This review highlights the role of rheology and process parameters in extrusion bioprinting and discusses qualitative and quantitative methods proposed to measure and define the printability of bioinks. Finally, an overview of key challenges and future trends in extrusion bioprinting is provided.

1. Introduction

Tissue engineering combines the principles of cell biology and engineering to develop functional substitutes to treat damaged tissues [1,2]. The crux of tissue engineering is that, mimicking the natural biology of the system facilitates more effective therapeutic strategies aimed at the repair and restoration of tissue function compared to inorganic interventions. Tissue engineering relies on implantable scaffolds, cells, and biological signals to achieve the structural and functional reconstruction of damaged tissues [3].

Scaffolds, which are porous three-dimensional structures, are designed to encourage and support the interaction between cells, signals, and the biological environment [4,5]. Scaffolds must be mechanically and geometrically similar to the native tissue, and aid in the formation of the extracellular matrix [6,7]. The porosity of the scaffold is crucial for the free movement of cells, nutrients, and biological waste [8]. Traditional scaffold fabrication processes such as electrospinning, solvent-casting, particle leaching, gas foaming, and compression molding are limited in their ability to realize pre-determined, well-defined 3D structures controllably [9–12]. Other technologies such as micro-molding allow the fabrication of biomimetic architectures, but they fail to recapitulate spatial cellular distribution [13,14]. Some other techniques used for bio-textile fabrication allow the creation of structures with biomimetic mechanical properties and cellular organization but engineering volumetric structures specific to a patient could be challenging.

Additive manufacturing has garnered attention as a fabrication method due to its ability to create patient-specific three-dimensional scaffolds and structures repeatedly [15,16]. In some cases, scaffolds can also be created using biological compounds native to a patient [17–20]. Bioprinting is one such technique that enables the three-dimensional deposition and sequential layering of cells encapsulated in biomaterials, a.k.a bioinks [21]. It is noteworthy that there is a bit of discrepancy on the definitions of bioprinting and bioinks (Table 1). However, in this work we refer to materials that can carry cells and biological materials as bioinks. Since bioprinting provides control over the spatial positioning of cells and biomaterials, it is an attractive technology for making engineered tissues and organs [22]. In the tissue engineering field (Fig. 1), digital representations of damaged anatomies are obtained through magnetic resonance imaging (MRI) or computerized tomography (CT). The obtained data is digitally processed to isolate and

* Corresponding author.
E-mail address: Iris.Rivero@rit.edu (I.V. Rivero).

https://doi.org/10.1016/j.bprint.2020.e00116
Received 18 August 2020; Received in revised form 1 November 2020; Accepted 17 November 2020

Table 1
Various proposed definitions for a bioink.

Definition of a bioink	Ref.
Combination of cells and biomaterials	[27,40–48]
A mixture of materials and cells	[49,50]
Printable material while printing cells	[51]
Cell-containing hydrogels	[52,53]
Materials that combine printability and cytocompatibility	[54,55]
Materials that mimic an ECM environment	[56,57]

create models of anatomical defects. The models are then sliced to create standard tessellation language (STL) files that serve as blueprints to manufacture implantable, cell-containing scaffolds. It is noteworthy that instead of the use of sophisticated imaging modalities, bioprinters can become portable, modular, and manual [23].

Extrusion-based bioprinting (EBB) has been the most popular bioprinting technique [24]. The widespread usage of EBB is due to its capability to print hydrogels of varying viscosities (30 mPa s to $>6 \times 10^7$ mPa s) and realize large-scale three-dimensional models (centimeter--scale) with high cell densities ($>10^8$ cells/mL) [25,26]. However, the resolution of the process is restricted, minimum feature sizes that can be created are in the range of 200–1000 μm, which makes it challenging to obtain intricate features that mimic biological tissues [27]. Additionally, there are tradeoffs between achieving good printing behavior and maintaining high cell viability. For instance, biomaterials (e.g. Pluronic [28], polyethylene glycol (PEG) [29], alginate [30] etc.) that possess favorable rheological and mechanical properties provide a sub-optimal environment for cells while other natural biomaterials (e.g. collagen [31], gelatin [32], chitosan [33], fibrin [34], decellularized extracellular matrix (dECM) [35] etc.) possessing favorable biological properties exhibit poor rheological and mechanical performance (Table 2). This property-level dichotomy is resolved by experimenting with the printing environment [36], bioink formulations [37], crosslinking mechanisms [38], and the use of sacrificial materials for enhanced mechanical and temporal stability of the bioprinted structures [39].

This paper reviews the role of rheological properties of bioinks in influencing the outcome of bioprinting and discusses strategies for achieving desirable rheological behavior. The role of printing parameters is also discussed in the context of print quality and cell viability. Additionally, methods utilized for the qualitative and quantitative assessment of bioink printability are discussed. Finally, an overview of the future trends in extrusion bioprinting is provided.

2. Mechano-rheological considerations

EBB uses a fluid-dispensing setup mounted on a robotic system that moves the extrusion head along computer-generated toolpaths [83]. However, if needed, the movement of the nozzle can also be manually controlled. Fluid dispensing is achieved using mechanical or pneumatic actuation, where the loaded bioink is pushed through a nozzle [24,84]. The normal force exerted by the downward motion of the plunger induces a rheological response from the bioink, which determines its flow through the nozzle. The flow response of a bioink is vital while developing and screening bioinks (Fig. 2). Herein, we discuss the role of rheological properties in influencing extrusion.

2.1. Viscosity

In bioprinting, viscosity is the resistance of a bioink to a deforming force [85]. Although EBB is used to print materials with a wide range of viscosities, there are competing objectives when it comes to the ideal viscosity [68]. For instance, high viscosity bioinks are readily extruded and can retain shape following extrusion. However, they require high deforming forces during extrusion, which can harm encapsulated cells [86,87]. Low viscosity bioinks can minimize nozzle-clogging and enable mixing of cells but cannot maintain shape following extrusion resulting in

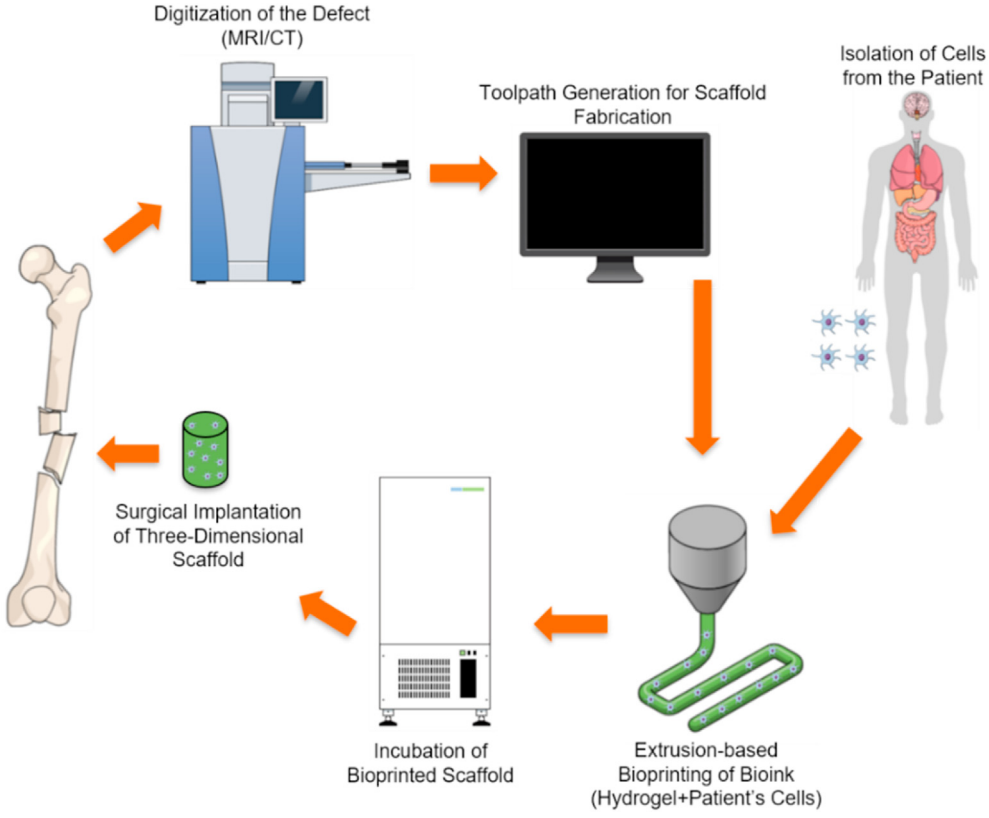

Fig. 1. Schematic representation of the various steps involved in an extrusion bioprinting-based tissue engineering approach. The presented workflow is divided into three distinct stages: pre-printing, printing, and post-printing.

Table 2
Ideal properties of bioinks for EBB.

Category	Ideal Properties of a bioink
Printing	Printability [33,41,44,48,55,58–68], Printing fidelity [52,65,69], Shape retention [61,62,70], Long-term shape fidelity [28,71], Formability [66]
Biological	Biocompatibility [41,49,56,60,62,66,72,73], Support cell migration, proliferation, differentiation & tissue generation [28,40,53,55,63,67,74], Cytocompatibility [27,33,50,54,60,67,72], Biodegradable [48,50,62,72,73], Protect cells from damage [49,75], Structural integrity in medium [76], Cell adhesion binding sites [77], Support formation of functional graft [74], Non-toxic [60]
Rheological	Shear-thinning [25,28,29,43,55,56,61,68,69,77–81], Quick shear recovery [28,29,43], Adjustable viscosity [25,45,58], Pseudoplasticity [77], Thixotropy [66,82], Substantial yield stress [43,79], Relatively high viscosity [80], Viscoelastic properties [70]
Physical	Mechanical strength [40,62,65,72,75], Rapid and tunable gelation [16,40,71,79], Mild crosslinking conditions [16,29,49,50,54,58,80], Stiffness [48,62], Tailorable mechanical properties [45,49], Cytocompatible gelation [68], Elasticity [58]
Other	Overall stability [48], Easy manipulation and handling [28]

poor feature definition [48]. Ideal bioinks for use in EBB need to demonstrate two properties related to viscosity. First, the ink is shear-thinning upon the application of a deforming force. Second, the ink's viscosity increases quickly after the removal of the force to facilitate shape retention [77,88,89].

2.1.1. Linear viscoelastic region

Rheological tests are conducted within the linear viscoelastic region (LVR), the boundary of which is marked by a critical strain or stress value. The LVR is identified using an amplitude sweep test where the load (stress or strain) on the sample is steadily increased while maintaining constant frequency.

The measured moduli (loss (G″) and storage (G′)) are plotted as functions of the applied load, and the critical value is chosen as the point beyond which G' departs from a constant value marking the onset of non-linearity (Fig. 2A). Chen et al. identified the LVR for magnesium phosphate-based bioinks (TMP-BG) to be within 0.4% strain using sweep tests conducted at 1 Hz [66]. Likewise, for gelatin/alginate bioinks, Ouyang et al. identified 0.1% strain to be within the LVR using an amplitude sweep performed at 1.5 Hz [40]. In general, once the LVR is found, subsequent rheological tests are conducted within that region [28,65].

2.1.2. Shear-thinning behavior

Bioinks developed for EBB show a reduction in viscosity when subjected to a deforming force (Fig. 2B). The degree of shear-thinning depends on the molecular structure of the material. To quantify shear-thinning, a frequency sweep is employed where the response of a bioink to changing frequencies is measured at a constant temperature for loads within the LVR. The steady-state viscosity (η) versus shear rate ($\dot{\gamma}$) plot is characterized by fitting the power law equation ($\eta = K\,\dot{\gamma}^{(n-1)}$) to deduce the values of the consistency index (K) and flow behavior index (n). According to Paxton et al., the printability window of a bioink is dependent almost entirely on its shear-thinning coefficients [41]. They demonstrated that pre-crosslinked alginate with a K-index value of 254 and n value of 0.307 had a wider printability window compared with uncrosslinked alginate that had values of 130 and 0.433, respectively. Li et al. also reported that all their tested hydrogels (alginate, chitosan, xanthan gum (XG), kappa-carrageenan (κCA), gelatin, and gelatin methacrylate (GelMA)) shear-thinned with $n < 1$ [89].

2.1.3. Viscosity-recovery behavior

Measuring viscosity-recovery behavior is crucial to understanding and predicting the ink's post extrusion viscosity-related behavior. After a reduction in viscosity during extrusion, it is essential that the viscosity of bioinks quickly increase after exiting the nozzle [25]. This behavior is known as thixotropy, a property that enables the reduction of viscosity upon the application of flow followed by its time-dependent recovery after the discontinuation of flow [90].

From an EBB perspective, faster recovery times are associated with the superior definition of features in a printed construct. A three-interval thixotropy test (3ITT) is employed for characterizing and quantifying the fluid's recovery behavior. In a three-interval test, time sweep experiments are conducted where the sample is subjected to successive cycles of low and high strains (Fig. 2C). Chen et al. performed a 3ITT for TMP-BG bioinks at low and high strains of 0.05% and 30%, respectively [66]. They noted that the ink recovered 92% of its original G′ in 0.5 h. Li et al. demonstrated the thixotropic behavior (>85% recovery) of cationic (alginate, XG, κCA) and anionic (gelatin, GelMA, chitosan) hydrogels using low and high shear rate values of 0.1 s^{-1} and 100 s^{-1}, respectively [89].

2.1.4. Modifying viscosity

Viscosities of bioinks are influenced by four factors, (a) temperature, (b) polymer concentration, (c) molecular interactions, and (d) molecular weight (MW) [27]. Several methods have been employed to alter the viscosities of bioinks to achieve high feature definition. For instance, Levato et al. used 1% w/v gellan gum (GG) to enhance the viscosity of GelMA [53]. The inclusion of GG did not impact the osteogenic

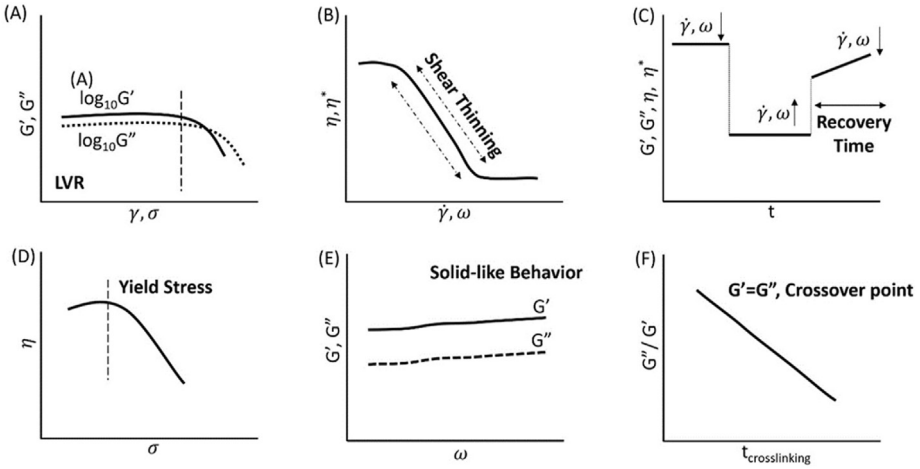

Fig. 2. Rheological properties to consider while developing and screening bioinks for EBB.

differentiation of stem cells but improved the printing behavior of GelMA. Kumar et al. increased the viscosity of furfuryl-gelatin through the addition of 1% w/v hyaluronic acid (HA) [56].

The addition of enhancers at minimal concentrations is crucial for not disturbing the crosslinking of bioinks [91]. Liu et al. showed that the viscosity of alginate increased with increasing κCA concentration (0.5–1.5% w/v). This improvement in viscoelastic property facilitated the stacking of bioinks with high fidelity without affecting biological function (Fig. 3(A-D)) [92]. Alcala-Orozco et al. enhanced the viscosity of GelMA using strontium nanoparticles (1.5 mg/mL) and demonstrated excellent shape retention (Fig. 3(E-F)) [93]. The presence of the nanoparticles encouraged the osteogenic differentiation of the cells. Cellulose nanofibers (CNFs) or nano-fibrillated cellulose (NFCs) are other alternatives for increasing the viscosity and enhancing the shear-thinning behavior of bioinks.

Markstedt et al. used NFCs to impart shear-thinning behavior to alginate hydrogels that formerly showed no shear-thinning behavior [94]. The viscosity of GelMA (0.02 Pa) was considerably improved (>400 Pa with 1% CNFs) via the addition of CNFs and produced high-fidelity structures (Fig. 3G-H) [95]. Laponite particles have also been used for incorporating shear thinning behavior in bioinks. The surfaces of these particles are negatively charged while the edges are

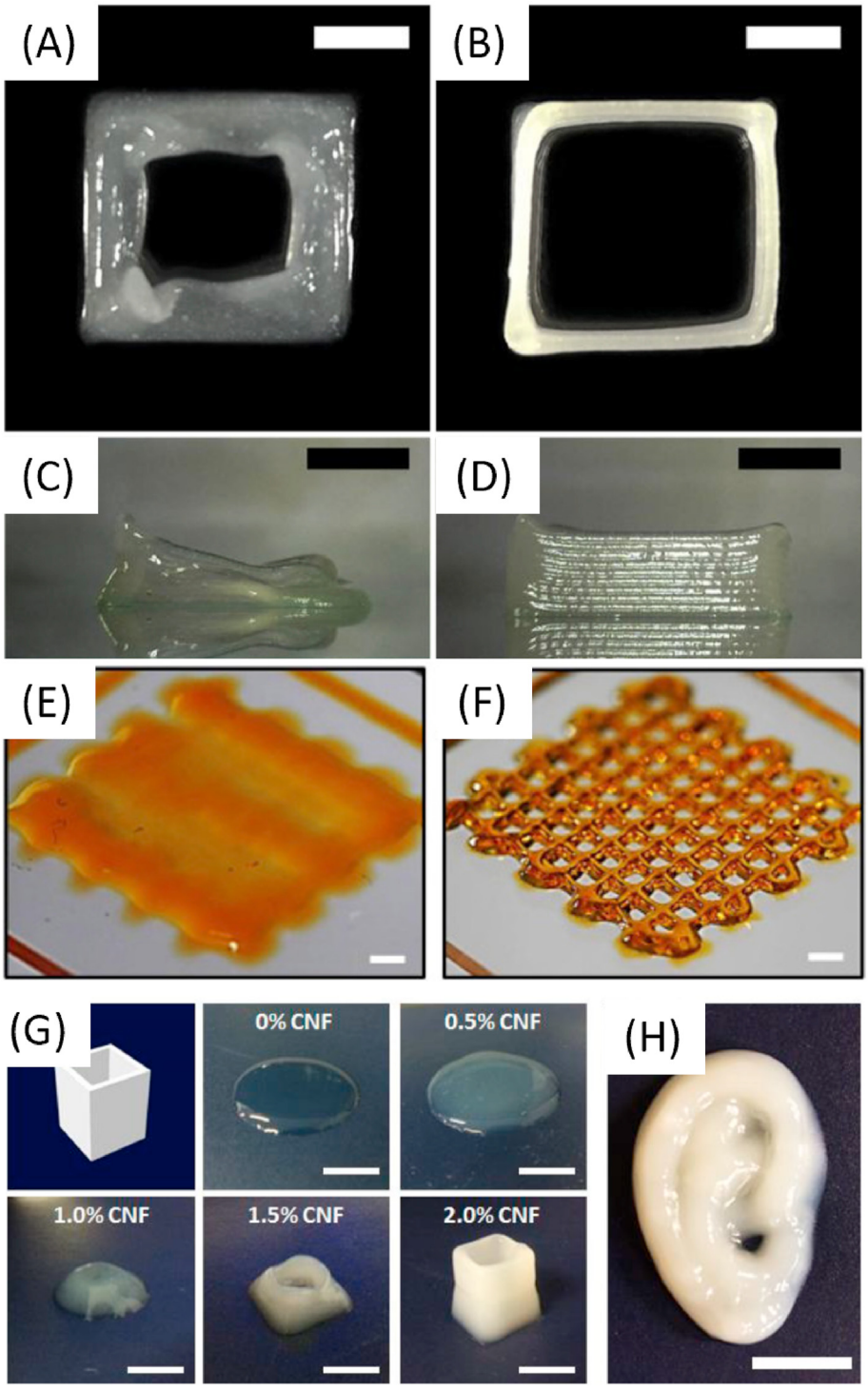

Fig. 3. The addition of viscosity enhancers can improve viscosity and printing behavior of bioinks. (A–D) The addition of κCA to alginate facilitated the stacking up of layers with high fidelity (Scale bars: 5 mm). Reproduced with permission [92], Copyright 2019, Elsevier. (E–F) Strontium nanoparticles acted as effective viscosity enhancers for a GelMA-based bioink and provided excellent pore and strut definition (Scale bars:1 mm). Reproduced with permission [93], Copyright 2020, Elsevier. (G–H) The addition of 2% CNFs to GelMA improved the viscosity of the ink resulting in the creation of stable hollow cube structures and other anatomical shapes [95], Copyright 2017, BioResoruces.

positively charged. This unique feature of Laponite particles provide an edge-rim electrostatic attraction. The colloidal network created through the addition of these particles is temporarily destroyed under an applied force and is rebuilt upon the removal of shear establishing the foundation for its shear-thinning behavior [96,97]. Pereira et al. modified the viscosity through the ionic crosslinking of pectin methacrylate (PECMA) before the deposition step [45]. Another popular strategy to enable the printing of low-viscosity bioinks is to perform deposition into a liquid/gel bath [48]. Loo et al. investigated the deposition of low-viscosity peptide-based bioinks into a salt solution to create noodle-like structures [71]. Since the liquid-bath is capable of supporting the printed construct, this strategy provides the choice of crosslinking gradually and greater flexibility during biofabrication [98].

2.2. Yield stress

In bioprinting, yield stress determines the force required to maintain continuous and smooth extrusion during deposition. Low yield stress hydrogels leak out of nozzles even without the application of force. When cells are suspended in a bioink, the yield stress helps maintain the homogeneity of the encapsulated cells [45]. Bioinks with low yield strength are prone to settling or phase separation of cells. While high viscosity bioinks may hold their shape in a bioprinted structure for a short period, inks with high yield strengths are better able to retain shape until the completion of crosslinking [99]. To measure yield stress, a stress ramp experiment is employed where the applied stress is linearly increased over time. Ideal bioinks will show a slight increase or plateaued response in viscosity, followed by a shear-thinning region that saturates at higher stresses (Fig. 2D). The stress corresponding to the viscosity peak is characterized as the yield stress. By plotting viscosity as a function of shear stress, the yield stress is identified as the stress value beyond which the material starts to flow.

Paxton et al. measured the yield stress of a series of alginate and alginate-gelatin bioinks. They remarked that a distinction could be made between printable and unprintable materials based on yield stress. Pre-crosslinked hydrogels showed excellent printability because of their relatively high yield stresses in comparison to unprintable inks [41]. Kiyotake et al. showed that the yield stress of their HA-based bioink increased with increasing polymer concentration. At 4 wt% of HA, the bioink showed yield stress of approximately 380 Pa, which was not significantly different from that of their control ink, Cellink Start® and therefore, yielded comparable structures (Fig. 4(A,C)) [100]. In general, inks with higher yield stresses produced shape-retaining structures. Mouser et al. also demonstrated that yield stress was the most important parameter to characterize printability and reported a positive correlation between yield stress and printability [101]. It should also be noted that high yield stresses may have detrimental effects on cells while initiating flow [102].

2.3. Complex modulus

Complex modulus of a viscoelastic material has two components – (a) G'', which is a measure of the stored energy in the elastic region, and (b) G'', a measure of the dissipated energy. Moduli is used to predict printability and understand the material's response to crosslinking stimuli [103]. When $G' > G''$, the bioink will show a gel-like behavior resulting in a stable system. When $G'' > G'$, the bioink will display a sol-like status, and the result is a mechanically inferior system incapable of providing high-definition post extrusion (Fig. 2E) [40].

The crossover point beyond which $G' > G''$ is considered the gelation point. The change in moduli during crosslinking can be monitored to identify the right printing conditions for a bioink [28]. Zhao et al. investigated the role of rheology in affecting cell survival rates of the A459 cells [104]. They identified a correlation between the rheological properties and cell survival and showed that the $G' < 382$ Pa was required to achieve a cell survival rate of 90%. Frequency sweep experiments are used to measure the moduli of bioinks. The frequency of oscillation for an applied load is progressively increased at constant temperature and amplitude G', G'', and complex viscosity (η^*) are plotted as functions of frequency and analyzed to classify the behavior of bioinks.

Gao et al. investigated the blending of gelatin and alginate to tailor rheological properties [105]. They identified a correlation between moduli and print quality and proposed that G''/G' values between 0.25 and 0.45 are required to strike a balance between printability and cell viability. Lee et al. compared the moduli of type A and type B GelMA before and after ultraviolet (UV) curing and observed that by having $G' > G''$, both the hydrogels were able to maintain their structural integrity after printing even at an uncured state [106]. Since the G' of type A

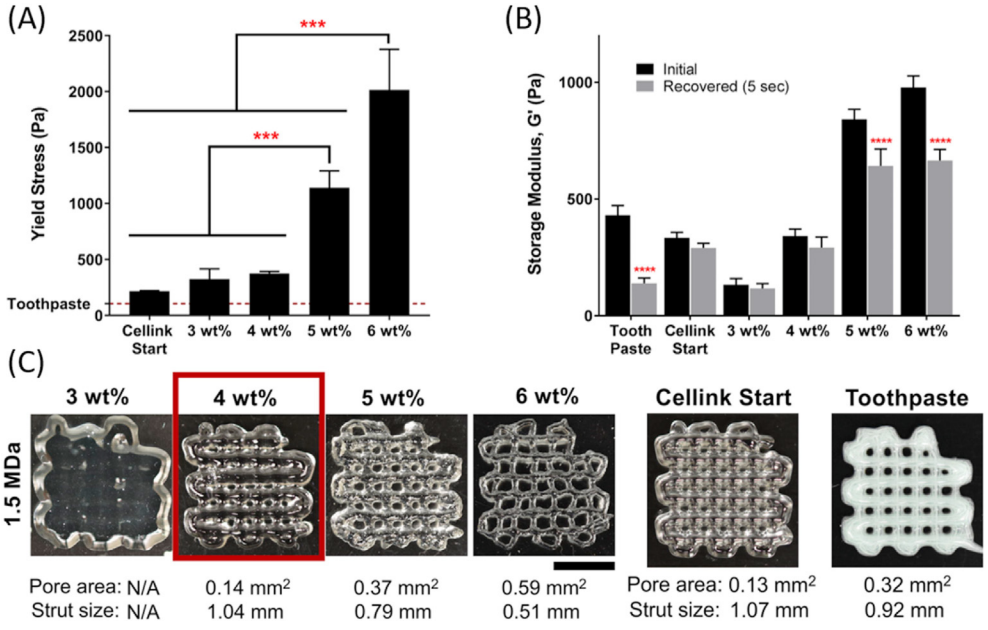

Fig. 4. (A–C) Influence of yield stress and storage modulus on bioprinting performance. The printing behavior of HA-based bioinks were analyzed with Cellink Start® and toothpaste serving as control inks (Scale bar: 5 mm). In general, high-viscosity materials with high yield stresses produced strucutres with good strand and pore definition. Reproduced with permission from Refs. [100], Copyright 2019, Elsevier.

GelMA was much higher than that of type B GelMA, the former was able to maintain better integrity at room temperature. Kesti et al. were able to minimize the risk of undesired gelation by selecting a 15% poly(N-isopropyl acrylamide) grafted to HA (HA-pNIPAAM) bioink which had a crossover point ($G' = G''$) at 29.7 °C (i.e., higher than ambient temperature) [25]. During recovery studies, Shi et al. observed $G' > G''$ at low strains in HA-biphosphonate-Ca^{2+} but the ink shear-thinned at higher strains such that $G'' > G'$. This behavior allowed for smooth extrusion followed by a quick recovery which was marked by a sudden increase in G' values upon removal of high strains [42]. Kiyotake et al. proposed that the minimum threshold of G' recovery must be at least 85% to achieve good printing behavior. 3 wt% and 4 wt% HA-based bioinks possessed recoveries >85% but the 4 wt% bioink was chosen for scaffold printing due to its higher viscosity which yielded square scaffolds with well-defined edges (Fig. 4) [100].

2.4. Loss factor

The loss factor ($tan\delta$) is defined as the ratio of G'' to G' and is used to characterize the stability of materials. The loss factor provides useful information about the state of crosslinking and the stability of a material system (Fig. 2F).

For example, while optimizing printing conditions for polyelectrolyte gelatin-chitosan hydrogels, Ng et al. formulated gels with varying concentrations of gelatin (2.5%, 5%, and 7.5% w/v). They characterized their rheology and printing behavior [107]. They used the loss factor as a metric to predict the printability of the gel and showed that the gels containing 5% and 7.5% of gelatin offered excellent shape fidelity.

Petta et al. investigated the correlation between the loss factor, extrudability, and printability [70]. According to them, bioinks with tanδ greater than 1 correspond to no shape retention. When tanδ is between 0.6 and 1, there is poor shape retention. When $tan\delta$ falls between 0.4 and 0.6, there is good extrudability and shape retention, and inks having $tan\delta$ values less than 0.4 were not extrudable. Likewise, Markstedt et al. predicted the stability of a family of alginate-NFCs bioinks [94]. They saw that all the bioinks consisting NFCs had tanδ greater than one which indicated gel-like behavior and resulted in mechanically stable prints.

2.5. Shear stress

The normal force created by the downward motion of the plunger is transformed into shear stress (τ) at the nozzle interface (Fig. 5A) [77]. Shear force at the nozzle must be monitored while printing cells. High shear forces can damage cells suspended in the bioink. In general, low shear forces are preferred for high cell survival rates [87,108]. Low viscosity bioinks that shear-thin, experience reduced shear forces due to the reduced resistance to flow and are preferred for cell printing. In addition to viscosity, nozzle geometry plays a vital role in determining the shear forces experienced by cells. The length of the printing nozzle needs to be carefully chosen, as long exposures to even low shear stresses could be detrimental to cells [109]. Ouyang et al. computed the maximum shear stress (τ_{max}) using the equation, $\tau = K\ \dot{\gamma}^{(n-1)}$, for an alginate-gelatin bioink and showed an exponential relationship between τ_{max} and cell viability [40]. Shear stresses lower than 100 Pa were required to obtain cell viability higher than 90% while printing stem cells. Muller et al. used fluid dynamics simulations to calculate τ_{max} and its correlation with cell survival [110]. In their study, needles exhibited two areas of high shear - one at the transition between the needle holder and needle tip, and another within the tip itself. Conical needles were better for minimizing shear stress as they had only one high shear zone located at the exit orifice.

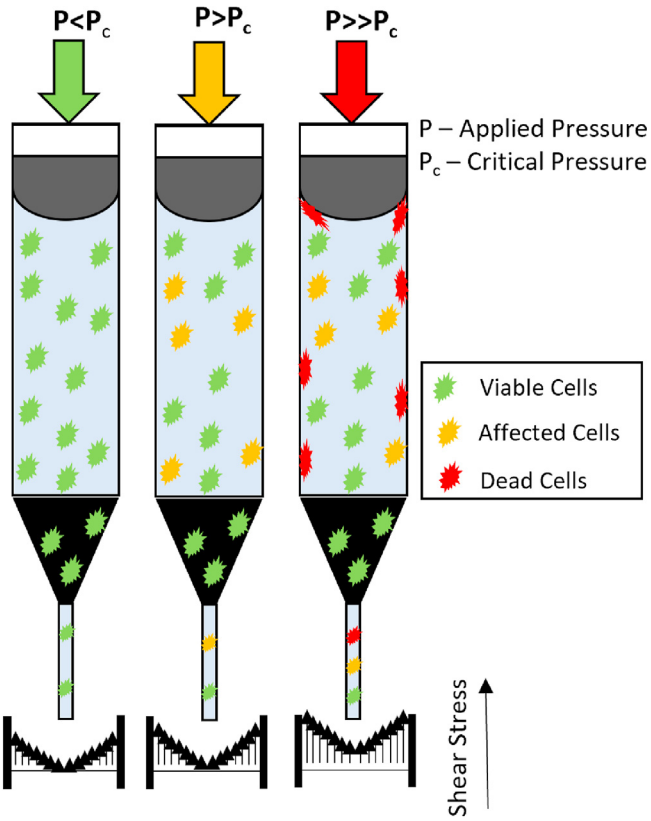

Fig. 5. Exposure to higher levels of shear stress can be detrimental to cellular health and negatively affect viability.

3. Extrusion parameter considerations

In EBB, printing happens in phases that occur sequentially, (Phase I) force application to initiate and maintain extrusion, (Phase II) extrusion and filament formation, (Phase III) 3D deposition controlled by the movement of the robotic arm, and (Phase IV) crosslinking of bioprinted constructs to ensure mechanical integrity (Fig. 6). This section of the paper will focus on the role of printing parameters in each stage and summarize approaches used for characterization and optimization.

3.1. Printing pressure

Most EBB processes use a pneumatic system to dispense bioinks through nozzles that move following a computer-generated toolpath. Pneumatic systems use compressed air to aid adequate extrusion. Printing pressure needs to be optimized to initiate the generation of continuous filaments during extrusion. The yield stress of the bioink determines the air pressure required to achieve extrusion. It is known that the applied air pressure needs to be sufficient to overcome the surface tension of the bioink. For a given bioink, low printing pressures can result in insufficient extrusion and cause discontinuities in the printed lines. Conversely, high pressures can result in unstable flow. Therefore, a range of pressures that produce continuous, stable, and uniform filaments needs to be identified. The air pressure range depends on yield stress, viscosity, nozzle translation speed, and nozzle geometry. Ahn et al. demonstrated that it was possible to achieve similar filament widths using different pressures by altering printing speed and bioink concentration. Higher pressures caused wider filaments when viscosity and

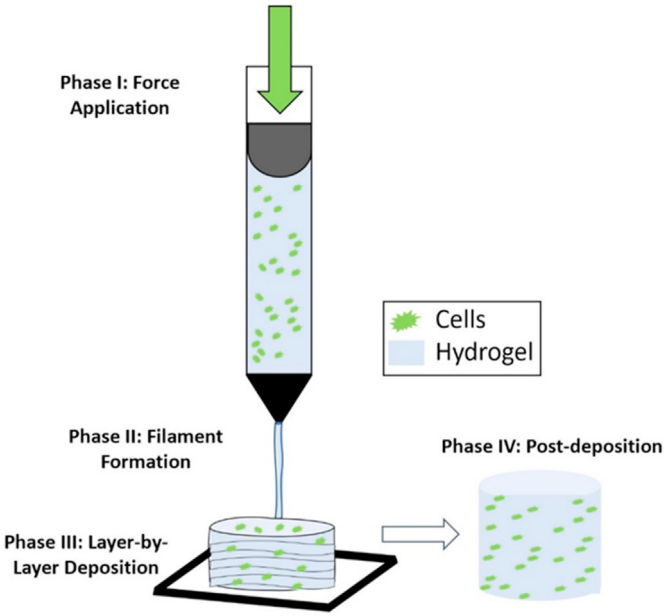

Fig. 6. Various phases of an EBB process.

printing speed was retained constant [64]. The correlation between viscosity and printing pressure was also confirmed by Yeo et al. in a study where different ratios of collagen and tannic acid (TA) (1–3 wt% of TA) needed different pressures to generate filaments with similar dimensions [60].

3.2. Printing speed

The movement of the nozzle along the x and y-axes during deposition creates 2D geometries, while movement along the z-axis creates 3D structures in a layer-by-layer manner. The speed at which the nozzle moves during deposition determines the geometrical characteristics of the deposited filaments. The print speed of the nozzle is chosen to approximately match the velocity of bioink flowing out of the nozzle. As extrusion pressure increases, the flow rate of ink through the nozzle increases, and the print speed must increase as well. If the print speed is higher than the velocity of ink exiting the nozzle, then the extruded filament is elongated and may result in discontinuities or inferior mechanical properties [44]. If the print speed is below the velocity of ink, then the ink spreads laterally to produce wider printed lines.

While optimizing an alginate-gelatin mixture, Webb et al. remarked that at higher printing pressures, the increase in printing speed had a more significant effect on strand width (Fig. 7A) [111]. At the faster printing speeds, adequate extrusion was not possible for some combinations of nozzle diameter and printing pressure. They observed a decrease in strand width, which was exponential with increasing print speed at higher pressures, but linear at lower pressures. The printing accuracy for these experiments was calculated using a parameter optimization index (Fig. 7B). Athirsala et al. demonstrated that for the same printing pressure, formulations with higher viscosities needed lower printing speeds than bioinks with lower viscosities [77]. When high viscosity bioinks were printed with high printing speeds, feature definition was affected at points where there was an abrupt change in the print direction. This resulted in curved edges rather than straight edges. In another study, Wilson et al. highlighted the importance of the tradeoff between printing speed and achievable resolution [61]. While printing a κCA-nanosilicates ink using a 350 μm nozzle, a lower printing speed (4 mm/s) resulted in strands with more excellent dimensional uniformity (369 ± 25 μm) than those achieved at higher speeds (8 mm/s).

3.3. Printing temperature

Since temperature influences the rheology of bioinks, determining the optimum print head and bed temperatures is crucial to obtaining smooth extrusion and deposition [28,40]. Additionally, the sensitivity of cells to their environment makes temperature an important factor in maintaining cell-viability [57]. Temperature is used to modify the rheology of a bioink to achieve greater control over printing. Some commonly used temperature-sensitive biomaterials include gelatin, collagen, GelMA, and Pluronic [112–114].

Many different methods to modulate flow behavior using temperature have been investigated. For instance, Ahn et al. investigated the effect of temperature on the printing resolution, mechanical properties, and cell viability of scaffolds printed using dECM bioinks [64]. By controlling the printing temperature at 36 °C, they obtained constructs with a high compressive modulus (approx. 4 kPa) due to heat-induced gelation of the bioink. Although the two-module heating setup did not significantly affect the biological performance, cell-laden constructs printed in temperature-monitored conditions possessed high-definition features. Zhao et al. used a holding temperature of 20 °C for gelatin bioinks to achieve G' and G'' in the range of 154–388 Pa and 10.4–17.9 Pa, respectively [104].

They modified the polymeric structure of gelatin-based inks to provide high cell viability during and after bioprinting. Koo et al. demonstrated the importance of temperature in modulating the G' of collagen bioinks [72]. By optimizing printing temperature, a high G' was achieved without denaturing the collagen. Additional mechanical stability was also imparted during printing. By including poly(N-isopropylacrylamide) grafted hyaluronan (HA-pNIPAAM) into the bioink, Kesti et al. bioprinted chondrocyte-containing scaffolds with excellent structural fidelity [25]. The formulated pNIPAAM-HA blend possessed a lower critical solution temperature between 25.7 °C and 29.7 °C. It was used as a support material to achieve quick gelation of a methacrylated-hyaluronan (HAMA) bioink printed at 37 °C. The addition of the sacrificial system was controlled to create a polymeric network that allowed the free diffusion of nutrients.

3.4. Nozzle design

Nozzle geometry determines the dimensions of extruded material. The slope and cross-section of nozzle channels are of interest as they influence the amount of shear experienced by the cells. Studies have investigated the relationships between shear stress and nozzle parameters such as length, cross-sectional geometry, inlet/outlet diameters, and convergence angle [44,66,74,108,115]. Nair et al. showed that lower pressures and larger nozzles provide a favorable environment for maintaining the high viability of endothelial cells [102]. Using a quantitative model, they predicted that shear stresses less than 20 kPa will lead to cell viabilities higher than 90%. Cell viability reduced to lower than 50% when stresses were more significant than 150 kPa while using 250 μm straight nozzles. Muller et al. investigated the effect of nozzle shape and diameter on cell proliferation and migration [74]. They observed that straight nozzles required higher extrusion pressures and imposed higher shear stresses on the cells during extrusion. They reported that there might be a maximum shear stress at which the cells lose their ability to migrate in the scaffold. Magalhaes et al. studied the effects of nozzle design on rheology using computational fluid dynamics [115]. The bioink was modeled as a non-Newtonian fluid, and the shear stresses and rates were evaluated for different nozzle designs using an inlet pressure of 0.2 MPa as the boundary condition. They concluded that the convergence angle and exit diameter are the most critical factors in balancing printing resolution and cell viability. Blaeser et al. investigated the effects of nozzle diameter and printing pressure on cell viability [108]. They observed that when fibroblasts were printed with low pressures (<5 kPa), a cell viability of 96% was maintained. At higher pressures, the cell viability dropped to a minimum of 76%. Their results reiterated the

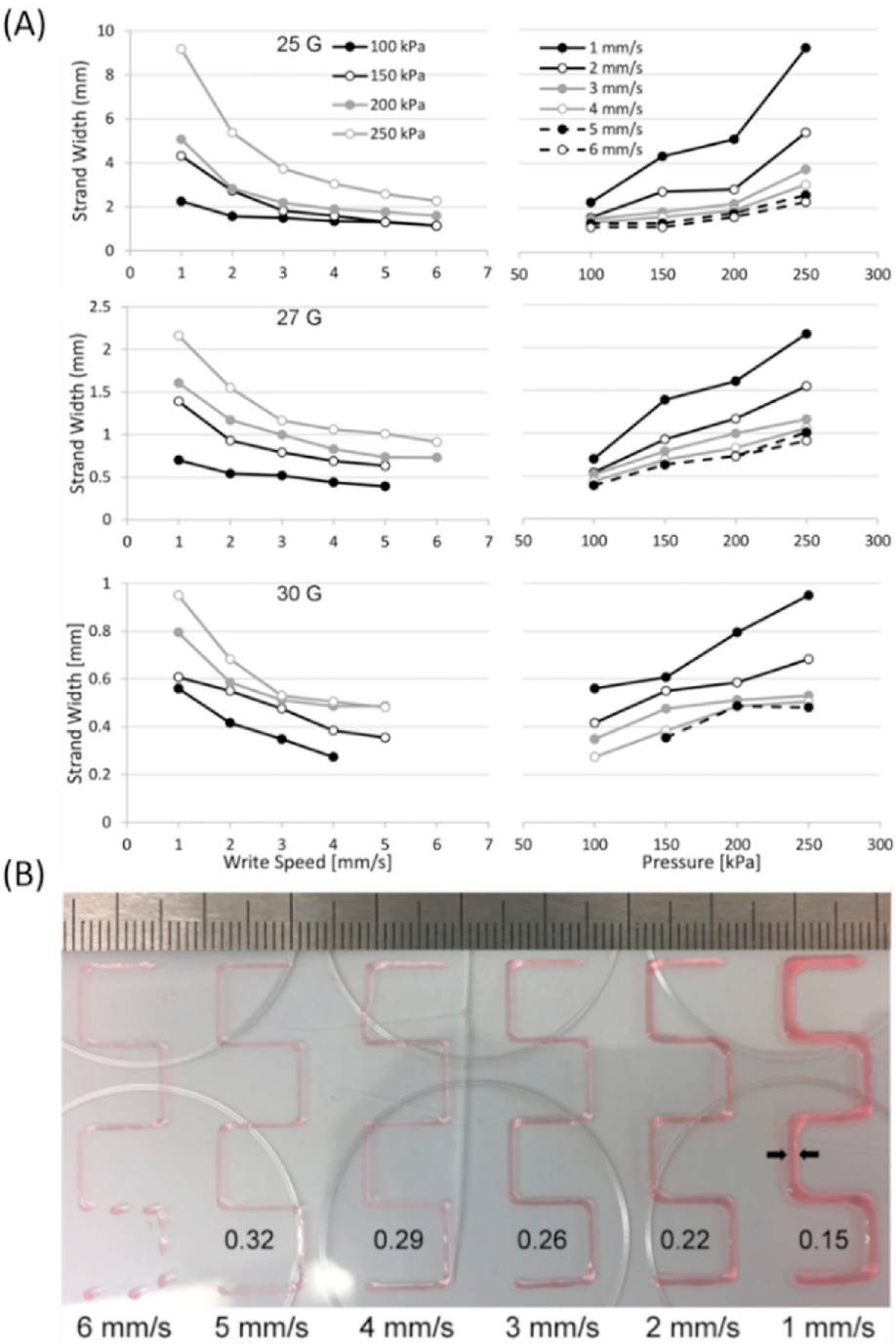

Fig. 7. (A–B) Effect of printing pressure and speed on the quality of the printed lines as demonstrated by Webb and co-authors. Reproduced with permission [111], Copyright 2017, Elsevier.

strong correlation between nozzle diameter and shear stress with wider nozzles minimizing the stresses experienced by cells.

3.5. *Crosslinking parameters*

Crosslinking is the process that strengthens the printed hydrogel construct by creating new bonds. The process is initiated and carried out using external stimuli [116]. Under sub-optimal conditions, the exposure of 3D constructs to crosslinking agents can be detrimental to cell viability. Therefore, crosslinking needs to be strategized to maximize structural integrity and cell viability [117]. There is an interest in devising crosslinking strategies to minimize the risk of toxicity and shape distortion [48, 118]. Muller et al. identified the crosslinking time for a blend of alginate-nanocellulose and alginate sulfate nanocellulose by monitoring the increase in G' as a function of the time [74]. They observed that 100 mM calcium chloride solution took 8 mins to crosslink alginate-nanocellulose, but 15 min to crosslink alginate sulfate-nanocellulose. Optimum crosslinking time of 12 mins was chosen, as G' values for both systems were equal at this point. Freeman et al. investigated the effect of ionic crosslinkers and their concentration on filament widths [75]. They observed that regardless of the choice of crosslinker ($CaCl_2$, $CaSO_4$, or $CaCO_3$), low MW (28,000 $gmol^{-1}$) alginate required an amount 2.5 times more than that needed by high MW alginate (75, 000 $gmol^{-1}$). They also observed that the mechanical properties of the crosslinked constructs were independent of the calcium source for low MW alginate. At the same time, $CaSO_4$ produced a significantly stiffer scaffold when used with the high MW bioink. Yeo et al.

investigated the role of TA concentration in improving the printing behavior of the hydrogel [60]. Higher levels (>3 wt%) of TA produced hydrogel networks with good G' values (>1500 Pa) and reduced the time and temperature required to crosslink. However, the cell viability of human adipose-derived stem cells (hASCs) was compromised (<90%). Therefore, an optimum concentration of 2 wt% was proposed to obtain high cell viability and printability. Pereira et al. showed that their developed PECMA hydrogel could undergo ionic crosslinking using calcium ions and UV light [45]. They demonstrated that dual-crosslinking hydrogels provides greater control by allowing the adjustment of rheological properties using calcium-mediated crosslinking before printing and UV photo-polymerizing after deposition. They printed different constructs within storage moduli ranging from 259 Pa to 3552 Pa. While post-crosslinking bioprinted structures require high viscosity bioinks, pre-crosslinking of low viscosity bioinks can lead to over-gelation which may require higher stresses for extrusion. To counter this problem, Connell et al. used an on-board light exposure strategy to perform rapid (<1 s) *in situ* photo-crosslinking of GelMA bioinks as they exit from the nozzle (Fig. 8) [119]. They also demonstrated a co-axial extrusion system, allowing for encapsulation of a soft or liquid core within the photo-crosslinked shell. This approach holds promise for the creation of free-standing structures without the need of support materials.

4. Evaluation of bioprinted structures

Comparing printed structure with the target computer-aided design (CAD) is essential as cell fate is extremely sensitive to geometrical and morphological cues from the scaffolds [120–122]. Various methods have been used to describe the geometric and dimensional concurrence of a printed structure with its intended design (Table 3). There has been an increase in the use of quantitative metrics to characterize print quality in describing this concurrence [45,59,61,123,124]. This section provides an overview of the different types of printability characterization.

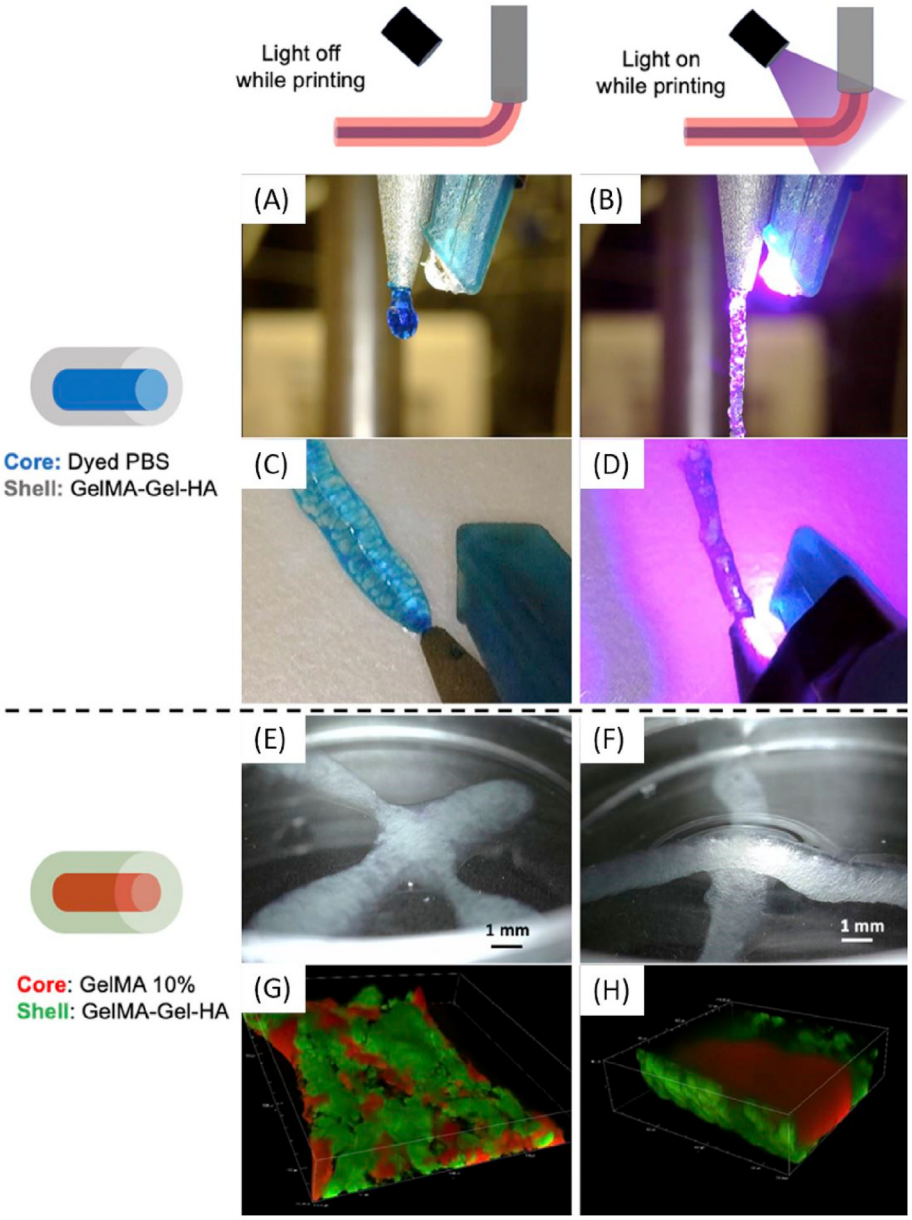

Fig. 8. Demonstration of *in situ* photo-crosslinking of GelMA-based bioinks during bioprinting (Scale bar: 1 mm). The extrusion of co-axial filaments resulted in the formation of droplets in the absence of light exposure (A, B, E, F) but on exposure to light (C, D, G, H), co-axial extrusion led to the creation of well-defined, uniform filaments. Reproduced with permission from Refs. [119], Copyright 2020, Elsevier.

Table 3
Various qualitative and quantitative metrics used for assessing print quality in EBB.

Hydrogel	Cells	Tissue/Application	Print Quality Metric	Printing Outcome	Ref.
Alginate	Acellular	Osteo/Adipogenesis	Spreading ratio (Printed line width ÷ Nozzle diameter)	2.5 times more crosslinker needed for low MW alginate in comparison to high MW alginate	[75]
GelMA, agarose, alginate	Mesenchymal stem cells (MSCs)	Cartilage	Spreading ratio	GelMA possessed best printability and line consistency	[69]
Agarose-collagen/chitosan	MSCs	Osteo/Adipogenesis	Droplet stacking (height, uniformity, stability, and diameter)	Agarose-collagen possessed good printability for differentiation into osteogenic and adipogenic fate	[33]
Alginate-NFCs	Acellular	Tissue Engineering (TE)	Grid-like pattern with straight paths, corners, and crossovers	Simulation predictions correlated well with printing results	[65]
TMP-BG	Acellular	TE	Line-width	Quick gelling capability created high definition grids	[66]
Alginate-honey	Acellular	TE	$\mathrm{Pr} = \frac{L^2}{16A}$; $\mathrm{C} = \frac{4\pi A}{L^2}$; where L refers to the perimeter and A refers to the area	5% alginate - (1–2%) honey yielded stable structres with high cell viability	[125]
Gelatin-alginate	Embryonic stem cells (ESCs)	TE	Circularity-based printability measurement	7.5% gelatin - 1% alginate printed at 30 °Cprovided high-quality structures with at least 90% viability	[40]
Collagen-riboflavin	Chondrocytes	TE	Dot footprint area, line measurements, square area error percentage	Concentration of riboflavin was optimized to balance viability, mechanical behavior. Gelation kinetics and rheological properties were pH-dependent	[103]
Cartilage acellular matrix (CAM)-silk	Acellular	Cartilage	Extruded cross-overs were analyzed	CAM-based inks showed good printability	[124]
Gelatin-alginate	Acellular	Soft Tissue Regeneration	Uniformity of strands and structural integrity of 3D structures based on height measurements	Gels with a loss factor between 0.25 and 0.45 showed best printability	[105]
Nanostructured Pluronic	Chondrocytes	TE	Qualitative assessment through images	Reversible thermo-gelling and good rheological properties allowed fabrication of stable, high-fidelity structures	[28]
Gelatin, alginate, chitosan, κCA, GelMA, XG	Acellular	TE	Pores assessed using circularity-based measurements	κCA2 and GelMA10 were found to be best oppositely charged gels and yielded high fidelity structures with cell viability greater than 96%	[89]
Dentin matrix-alginate	Acellular	Regenerative dentistry	X,Y, and Z print accuracy with respect to design parameters	High viability (>90%) and reproducible bioprinting achieved with 1:1 alginate-dentin	[77]
Agarose-alginate	Chondrocytes	TE	Normalized print parameter by analyzing overlaid images of strands	Alginate-agarose provided best printed structures with 75% cell viability	[81]
Alginate-polyvinyl alcohol (PVA)-hydroxyapatite (HAp)	MC3T3 cells	TE	Photograph-based qualitative analysis	2.5% alginate + 0.15% Na_2HPO_4 20% $CaSO_4$ + 2.5% HAp printed with high fidelity	[123]
Gelatin Type A and B	Human hepatocarcinoma cells	Regeneration therapy	Line width for comparing different gels and identifying process parameters	GelMA inks possessed good mechanical integrity and 80% viability	[49]
dECM	Cardiac progenitor cells	Cardiac TE	Line printing for parameter optimization	Structures were printed with high fidelity and crosslinked with UV and temperature	[88]
Collagen-polycaprolactone (PCL)	Rabbit articular chondrocytes (RbACs)	TE	Circularity-based measurements	With optimal temperature-controlled printing and crosslinking conditions, structures for *in vivo* applications were fabricated	[72]
PCL-dECM; PCL-alginate	Chondrocytes and pre-osteoblasts	TE	Line width measurement for parameter optimization	PCL-dECM hybrid scaffolds were fabricated for large-volume cell-printed constructs	[126]
Laponite-alginate-methylcellulose	MSCs	Skeletal TE	Qualitative image-based assessment	(3-3-3) Laponite-alginate-methylcellulose was chosen as the optimal formulation and allowed stacking of more than 25 layers with >75% viability	[52]
HAMA-HA-pNIPAAM	Chondrocytes	Cartilage TE	Line printing of optimization	HAMA-HA-pNIPAAM yielded structures with long term stablility and 91% viability	[25]
Alginate-NFCs	Human nesoseptal chondrocytes	Cartilage TE	Line width measurements	High viability and large-scale constructs were printed with 86% viability at Day 7	[94]
Vanadyl-chitosan catechol (V-CS-C)	L929 fibroblasts	TE	Manual extrusion into serum-containing media	V-CS-C showed well-defined grid printing capability with 89% viability	[127]
Phage-RGD/alginate	MC3T3-E1 cells	TE	Qualitative imaging and inspection	Alginate-10% RGD-phage showed good formalbility with well-defined pores and high cell viability	[50]
eADF4-(C16) silk solution	Human fibroblasts	TE	Qualitative imaging and inspection	Scaffolds showed high structural integrity and printed up to 16 layers with a construct depth of 3 mm	[54]
CNFs/GelMA	NIH 3T3 cells	TE	Stability of hollow cube was checked qualitatively	GelMA/CNFs yielded a high-fidelity human ear structure and showed high metabolic activity after 7 days	[95]
HA-Biophosphate-Ca^{2+}	MG-63, hASCs	Omnidirectional bioprinting	Strut-size analysis	Porous cell-laden scaffolds with high cell viability were fabricated	[42]
Alginate/alginate-sulfate	MC3T3-E1 cells	TE	Qualitative imaging and inspection		[59]

(*continued on next page*)

Table 3 (*continued*)

Hydrogel	Cells	Tissue/Application	Print Quality Metric	Printing Outcome	Ref.
				3% alginate - 1% alginate-sulfate showed uniform pore forming ability with high viability	
Collagen-TA	hASCs, pre-osteoblasts	TE	Line inspection	Optimal concentration of crosslinker was crucial in obtaining high fidelity and viability structures	[60]
κCA-nanosilicates	MC3T3-E1 cells	TE	Extruded fiber diameter	Complex structures fabricated with high viability	[61]
PECMA	Fibroblasts	Dermal tissue engineering	Filament formation was observed to optimize crosslinking	Dual crosslinking (ionic and UV) allowed fabrication of stable structures with tunable rheological properties	[45]
Lysine-containing hexapeptides	Human stem cells	Screening, diagnosis, tissue engineering	Droplet array printing	Hydrogels were printed as disks with high biocompatibility and stability.	[71]
Alginate-gelatin	A459 cell line for cancerous lung tissue in humans	TE	Qualitative image assessment of grids	Holding time and temperature were used to tune rheology. G′ of 154–388 Pa is required to facilitate shape fidelity and a clear contour.	[104]
GG-PEGDA	Bone marrow stromal cells (BMSCs) and MC3T3-E1 cells	Tissue and organ printing	Shape of filament and separating distance. Fidelity based on mesh area, height of the cylinder, and angle deviation of pentagram structures	1.5% GG - 10% PEGDA allowed the fabrication of human-scale constructs with high fidelity, stability and cell viability	[29]
Oxidized alginate	hASCs	TE	Normalized X and Y dimensional change.	5–15% oxidized alginate was suitable for high fidelity printing and cell viability	[63]
Tyramine HA derivate	Acellular	TE	Filament width for ink selection	Loss factor of 0.5–0.6 displayed best printability	[128]
Chitosan-Polyethylene oxide-Glycerol phosphate-Zinc oxide nanoparticles	Acellular	TE/Antimicrobial	Spreading ratio	Optimal printing parameters were identified by calculating the spreading ratio at different printing regimes	[91]

4.1. Line-based measurements

The measurement of printed lines is a common way to assess print quality in bioprinting. The ratio of printed filament width to the inner diameter of the extrusion nozzle, known as the spreading ratio, is a simple way to describe print quality [64,67]. Freeman et al. used the spreading ratio to examine the effects of molecular weight, crosslinking ratio, and gelling conditions on the quality of printing [75]. Spreading ratios close to one were indicative of excellent printing and used to identify optimum printing parameters for alginate bioinks. Li et al. used the spreading ratio to compare the printability of different hydrogels (alginate, agarose, PEGMA, and GelMA) for the fabrication of scaffolds for cartilage regeneration [69]. GelMA possessed the lowest spreading ratio (1.43 ± 0.36) and was more consistent than alginate, agarose, and a commercially available PEGMA hydrogel.

A few pioneering studies have developed sophisticated protocols for characterizing the quality of a printed line. Lopez-Marcial et al. developed a custom-written algorithm capable of overlaying CAD models with

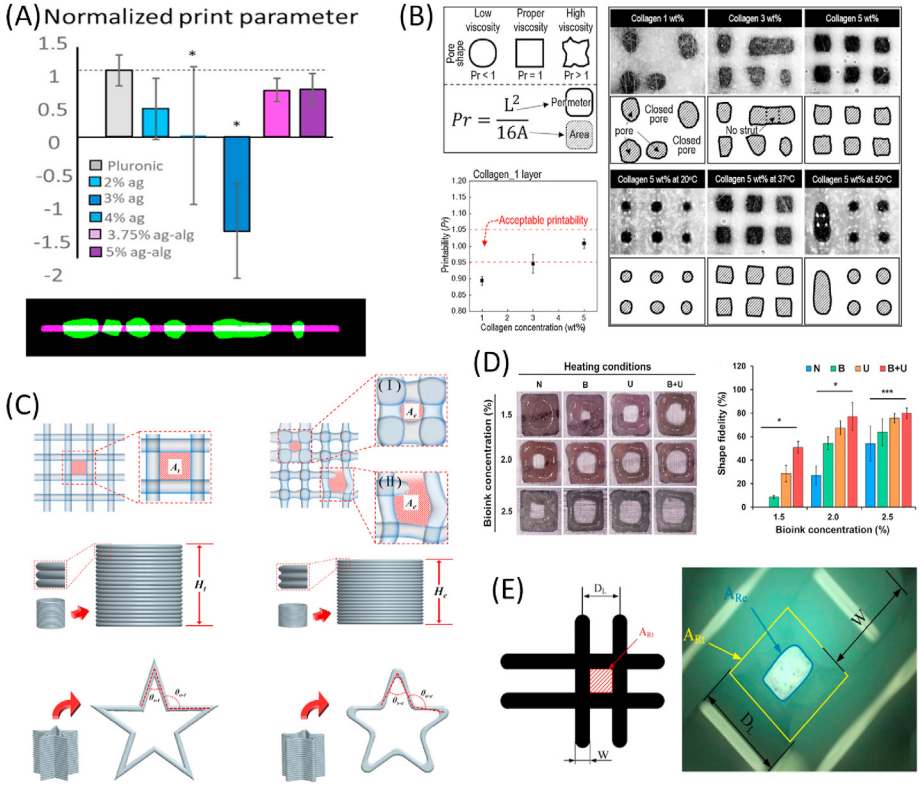

Fig. 9. Various quantitative methods used to describe print quality. (A) Lopez-Marcial et al. overlaid CAD models with pictures of printed constructs and calculated a normalized printing parameter to estimate print quality. The custom-written code separated gel and model pixels into one of three groups: gel pixels that do not overlap with the model (green), model pixels that are not covered by the printed gel (magenta) and overlapping pixels (white). Reproduced with permission from Ref. [81], Copyright 2018, ACS Publications. (B) Koo et al. identified printable concentrations of collagen bioinks by classifying printed structures based on the quality of their pores. Reproduced with permission from Ref. [72], Copyright 2018, Elsevier. (C) Wu et al. proposed the use of a lattice matrix, thin-walled tube, and pentagram as practical shapes for evaluating the printability of a bioink. Reproduced with permission from Ref. [29], Copyright 2018, Elsevier. (D) Ahn et al. used a shape fidelity parameter calculated based on theoretical and experimental empty space to compare the effectiveness of heating modules while printing dECM-based bioink. Reproduced with permission from Ref. [64], Copyright 2017, Nature Research. (E) He et al. proposed the use of a variable for the diffusion rate calculated based on the measurement of pores. Reproduced with permission from Ref. [129], Copyright 2016, Nature Research. (For interpretation of the references to colour in this figure legend, the reader is referred to the Web version of this article.)

pictures of printed constructs [81]. They calculated a normalized printing parameter that was defined as the percentage difference between the correctly placed pixels and incorrectly placed pixels (Fig. 9A). The calculated parameter was used to compare different hydrogels to balance print fidelity and cell viability of chondrocytes. The 5% agarose-alginate bioinks were ideal for cell printing as they maintained great shape fidelity and acceptable levels of shear force during printing.

Ribeiro et al. proposed the use of two different tests to describe the shape fidelity of the printed structures [43]. Their tests consisted of a filament collapse test for assessing the deflection of suspended filaments and a filament fusion test for characterizing x-y resolution of filaments. They compared hydrogels containing various concentrations of PEG and poloxamer 407. Based on rheology and dimensional measurements, they concluded that yield stress could be used to predict filament formation and estimate fidelity. Gao et al. proposed the use of a uniformity ratio, which was defined as the ratio of printed line width to the width of a perfectly uniform strand [105]. Using various combinations of alginate-gelatin, they demonstrated that bioinks with G''/G' values of $\geq$0.43 gave uniformity ratios close to one, which was indicative of smooth and uniform lines.

4.2. Pore-based measurements

Since porosity plays a crucial role in determining the performance of a scaffold, studies have investigated the morphology of pores to describe print quality. Lee et al. printed alginate bioinks consisting of different concentrations of M13 bacteriophage, a filamentous virus used as a biomaterial [50]. They evaluated the fidelity of pores generated from these bioinks utilizing the ratio of the experimental pore area to the theoretical pore area. They identified the concentration of phage (10 wt %) to be included in the alginate hydrogel without compromising the definition of pores in the scaffolds. Ouyang et al. introduced a printability metric, Pr, to determine the fidelity of interconnected channels printed using alginate-gelatin inks [40]. They showed that 7.5% gelatin - 1% alginate produced consistent pores (Pr ~ 0.9–1.1) when printed at 27.5 °C or 30 °C. When the bioinks were under-gelled (Pr $<$ 1), they produced pores with chamfers indicating the fusion of subsequent layers. Over-gelled (Pr $>$ 1) bioinks produced fractured filaments and irregular pores. Koo et al. used a circularity-based metric to study the temperature-dependent printing behavior of collagen bioinks by printing lattices (Fig. 9B) [72]. They reported that 5 wt% collagen at 37 °C was suitable for scaffold fabrication, as it printed well-developed struts with square pores and possessed Pr values in the printable region (Pr ~ 0.95–1.05). Athirsala et al. compared the fidelity of lattices with square pores bioprinted using different concentrations of alginate-dentin bioinks at different printing speeds [77]. The dimensions of the pores in the printed lattices were measured along x-y and z-planes and were represented as a percentage of concurrence with the design specification. The printing accuracy in the z-plane decreased when the overall viscosity of the formulation was lowered.

4.3. Other measurements

TE scaffolds are built as porous structures to facilitate the transfer of biological nutrients and oxygen during regeneration [5]. Therefore, grid-like pores are often bioprinted and measured while assessing the printability of novel bioink formulations. Gohl et al. proposed the use of a grid-like structure consisting of straight paths, corners, and cross-overs as a standardized design to characterize the printability of bioinks [65]. Wu et al. proposed the printing and measuring of three distinct structures, a lattice matrix, a thin-walled tube, and a pentagram to quantify the printability of a bioink (Fig. 9C) [29]. The fidelity of the lattice was calculated as the ratio of pore area in experiments to the pore area in theory. The fidelity of the thin-walled tube was calculated as the height of the printed construct divided by the height of the designed construct. The fidelity of the pentagram was calculated as the deviation of angles in the printed structure from its theoretical counterpart. Based on all the three metrics, hydrogel consisting of 1.5 wt% GG and 10 wt% PEGDA was chosen as the ink with the best printing behavior and used to print cell-laden scaffolds. Diamantides et al. deposited droplets of the same volumes of collagen with differing concentrations of riboflavin [103]. The dot print areas were measured and compared after 10 s of UV exposure. It was seen that a higher level of collagen (12 mg/mL) printed dots were 16–28% smaller than those printed with lower concentrations (4 mg/mL) and indicated an improvement in printability with increasing collagen concentration. They concluded that the best predictor of bioink printability is the storage modulus of the bioink during deposition. Gao et al. introduced a quantifiable metric known as structural integrity, which was defined as the ratio of the height of a printed cylinder to that of the designed cylinders [105]. They saw that the values of structural integrity decreased with increasing loss factor values of alginate-gelatin bioinks. Specifically, the structures began to collapse inward due to lack of mechanical stability. Ahn et al. printed hollow-shaped squares and estimated the printability of dECM bioinks using a shape fidelity parameter which is given by the ratio of the area of real empty space to the area of the theoretical empty space (Fig. 9D) [64]. They observed that the use of two heating modules to maintain printing temperature close to 37 °C and higher concentrations were key factors in obtaining well-defined structures. In another study, the measured metric for printability was diffusion rate, defined as the percentage difference between the theoretical and actual pore area [129]. They showed that diffusion of hydrogels causes the pore area to become irregular (Fig. 9E). This diffusion can be mitigated by increasing the distance between the lines in the lattice.

5. Modeling and computer simulation

Bioinks containing cells can be expensive, and printing trials are time-consuming. As a complement to experiments, a number of studies have relied on modeling and simulation for optimizing and predicting rheological, mechanical, and biological performance of bioinks. Gohl et al. presented the use of a computational fluid dynamics (CFD) simulation tool, IPS IBOFlow, to predict results in hydrogel printing [65]. Viscoelastic and surface tension models were used to simulate the deposition of CNFs-based bioinks.

The rheology of the bioinks was modeled using a linear Phan-Thien-Tanner model [130], and the surface tension forces were predicted using the continuum surface force method [131]. The ability to simulate 3D bioprinting of inks with distinct differences in viscoelastic properties showed that the tool can be utilized for a wide range of viscoelastic solutions and hydrogels. Muller et al. performed fluid flow simulations in COMSOL and fluid volume modeling in SolidWorks to predict the distribution of shear stresses in straight and conical printing nozzles [74]. The rotational symmetry of the printing geometries allowed the creation of 2D models for the COMSOL simulation. The simulations revealed differences between the straight and conical needle geometries in terms of the location of high shear areas. They speculated that in the future, optimized needle designs for a specific bioink might become a necessity to reduce the shear stresses and to maintain the well-being of cells while still being able to print at high resolution. Holzl et al. created a representative volume element model in which volume elements having a side length of 150 μm were used to represent hydrogels with different cell densities [27]. The encapsulated cells were modeled as 30 μm diameter solid spheres having Young's modulus of 1.5 kPa. The model allowed mechanical properties of hydrogels to be estimated at different cell densities (6.14–15 million/mL) and distributions (corner, cluster, and random). The experimental and finite element simulation results from ABAQUS showed that higher cell densities reduced the moduli of the hydrogel.

6. Future of bioprinting

Bioprinting technologies have significantly advanced in the past decade, and numerous breakthroughs have helped improve manufacturing processes, materials, modeling, and simulation capabilities. Nevertheless, as a relatively new technology in its early stages, there is a long way to go for bioprinting to achieve its ultimate goal – the production of fully functional human organs. This section focuses on the challenges and future trends to be expected in this field. We first highlight the trends in multi-material printing and high throughput printing, and *in situ* bioprinting followed by some future considerations for the computer modeling, simulation, and inspection of bioprinting processes.

6.1. Multi-material printing and process scaling

While the bulk of this review has focused on EBB materials and processes, biological constructs of practical significance inevitably require the printing of multiple materials. A brute force approach is to print each distinct material through its own dedicated nozzle. This approach is feasible for lab-scale demonstrations; however, arrays of nozzles dedicated to individual materials can require a great deal of space in relation to the size of the part that can be printed. An alternative approach is to independently pump individual bioinks through a manifold or microfluidic chamber that leads to a single extrusion nozzle [132]. By turning individual pumps on or off at the appropriate times, the composition of ink exiting the nozzle at a given 3D location can be varied. Liu et al. proposed a seven-material single-nozzle EBB configuration that demonstrates this concept, as seen in Fig. 10 [133]. This approach allows one to spatially vary the bioink composition throughout the 3D volume of a printed construct.

For purposes of scaling EBB for higher throughput than what is possible with a single nozzle, Skylar-Scott et al. describe an interesting technique in which 0D, 1D, or 2D arrays of nozzles can be fed by a single syringe pump per material [134]. The temporal pulse sequences for each material pump dictates what material exits all nozzles in the array at a given time. Fig. 11 shows a 4 × 4 array of nozzles (16 nozzles) being fed by four material pumps. While this type of configuration has a much higher material deposition rate than a single nozzle, the same material composition exits each nozzle in the array at any given moment in time. For high throughput EBB, multi-nozzle techniques that permit each nozzle to independently vary bioink composition as a function of 3D location will be needed to provide the greatest combination of speed, material flexibility, and geometric complexity.

6.2. In situ extrusion bioprinting

Bioprinting is capable of fabricating patient-specific implants that match the anatomy of the defect. However, surgical approaches treating tissue injuries typically involve a debridement step to remove damaged tissues or foreign objects from the surgical site. Therefore, predetermination of the geometry and scale of the defect to be treated may not be entirely known. Besides, the resolution of CT and MRI scans places a limit on the attainable fit. *In situ* bioprinting involves the direct printing of bioinks into defect sites to repair damaged tissues in a clinical setting [135,136]. This new paradigm functions on the premise that substitute tissues need not be fabricated externally but can be created directly within a defect site. While *in situ* inkjet bioprinting has been extremely popular for treating skin defects [137–139], the extrusion method has been applied for skin and cartilage repairs. Connell et al. fabricated a handheld extrusion system (Biopen) consisting of a pneumatic system that controls the extrusion of two bioinks [140]. The extrusion from both the bioink chambers and the attached UV curing system was independently controlled via foot pedals. *In vitro* experiments showed that GelMA/HAMA bioinks containing adipose-derived stem cells maintained high viability (>97%) after printing. Subsequently, they incorporated a multi-inlet extruder nozzle and a motorized extrusion system. They used the upgraded version to repair stifle joints (sheep) in a pre-clinical setting [141]. Their results demonstrated that defects treated

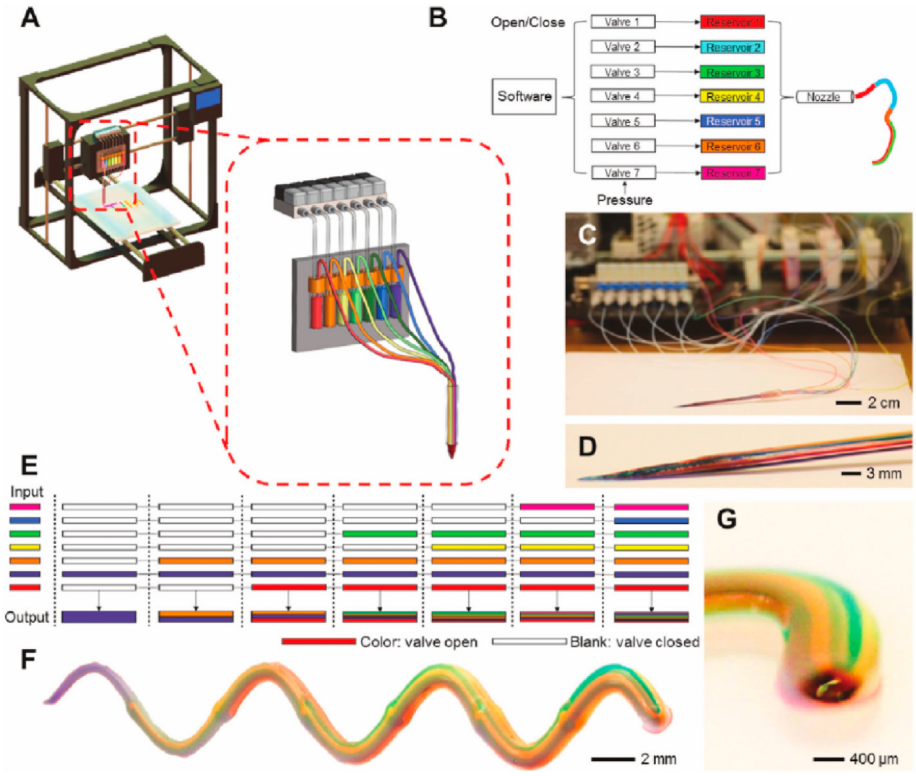

Fig. 10. Concept of a digitally tunable multi-material extrusion-based bioprinter. The proposed system is designed to deposit multiple coded bioinks rapidly with hassle-free switching among different reservoirs fabricating complex biological constructs. Reproduced with permission from Ref. [133], Copyright 2016, Wiley.

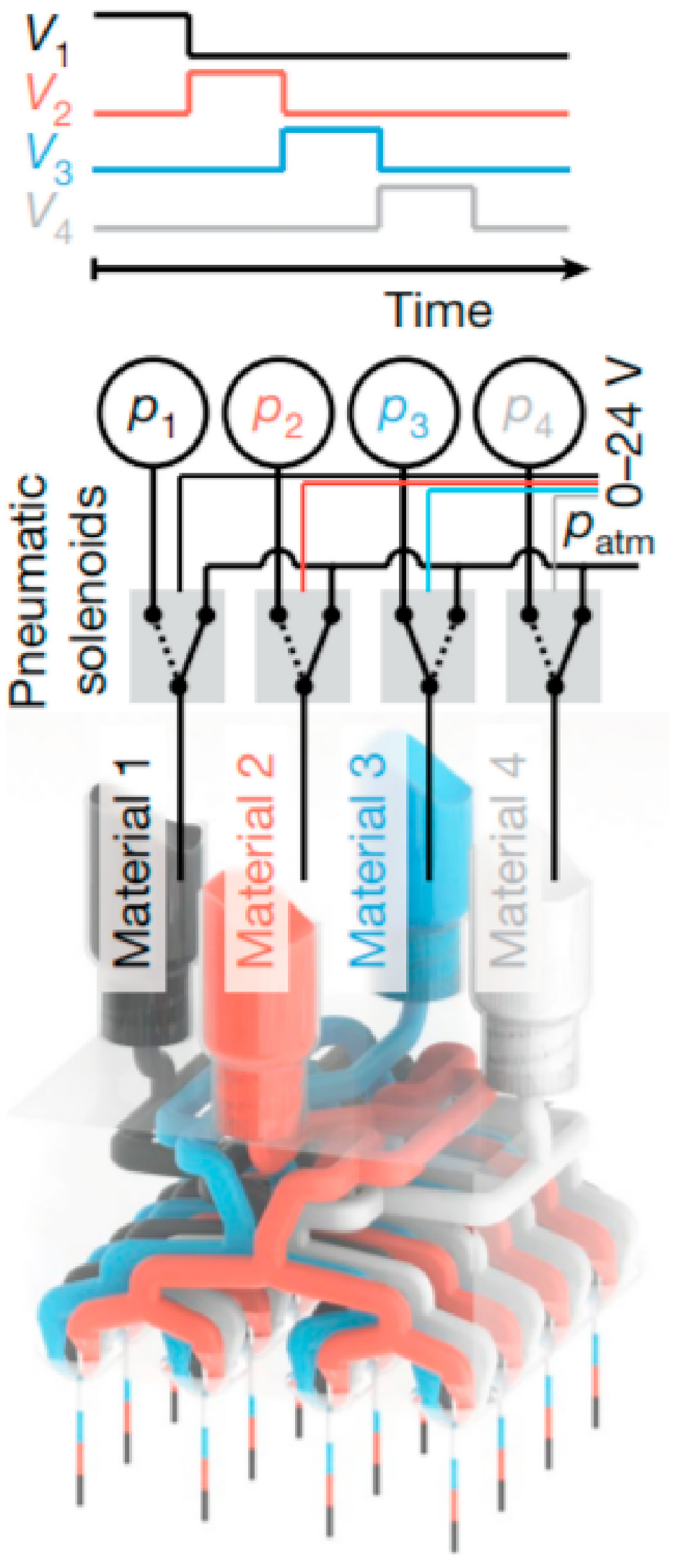

Fig. 11. Concept of a multi-material multi-nozzle (MM3D) printer for process scale-up. The MM3D system is capable of generating voxelated soft matter that combines multi-material switching for creating complex shapes with multi-nozzle printing for shorter build times. The structures are created in a voxel-by-voxel manner. Reproduced with permission from Ref. [134], Copyright 2019, Nature Research.

with *in situ* bioprinting had superior characteristics than controls and even showed the formation of hyaline-like cartilage. Hakimi et al. developed a portable handheld extrusion printer and printed alginate- and fibrin-based layered hydrogel sheets onto inclined surfaces in murine and porcine wound models (Fig. 12 (A-B)) [142]. After 20 days, it was seen that the bioprinted sheets did not inhibit re-epithelialization or wound granulation. Material considerations for *in situ* printing are similar to that of traditional EBB. Shear thinning property, stiffness, diffusivity, cell compatibility, biodegradability, and quick gelation of the bioink play a key role in the success of the approach. In the future, the integration of artificial intelligence or machine learning systems for parameter selection and high-resolution scanning will be essential to ensure the mainstream adaption of this technology. Finally, any concerns regarding sterility will also have to be addressed. In another example, Russel et al. developed a portable pen-like printer and used it for the deposition of GelMA-based bioinks for the treatment of volumetric muscle loss (VML) (Fig. 12 (C–F)) [23]. The *in situ* printing and crosslinking of scaffolds allowed proper adhesion to the native tissue and avoided scaffold dislocation after surgery. After 28 days of implantation, the *in situ* printed scaffolds resulted in significant hypertrophy.

6.3. Modeling for complex geometry

As bioprinted tissue constructs become increasingly complex, currently available commercial CAD packages struggle to support the modeling of biomimetic models. Since the adoption of CAD packages in the 1960s, 3D shape representation models have been modified and improved to suit conventional manufacturing processes such as machining, casting, and metal forming. Built on parametric shape representative models, existing CAD packages are deficient in their capabilities to create, define, and represent geometrically complex shapes. Apart from being unstable, inefficient, and highly memory-consuming, CAD packages assume that part volumes consist of a single material. The ability to model multi-material tissue models is lacking. These limitations have deprived researchers and clinicians of appropriately representing constructs to be tested for clinical use. To address this challenge, new shape representations are expected to be developed and popularized. Some shape representations currently under development include voxel [143], Ray-rep [144], point-sampled geometry [145], VRep, and some other implicit representations such as FRep and distance field [146]. These computational methods are developed to improve computational stability and efficiency. For example, Fig. 13 shows a computational tool for designing and optimizing customized arm casts with complex geometry and optimized structurality, built upon signed distance field and topology optimization [147,148]. Advancements along these lines will be critical for bioprinting to achieve its ultimate clinical goal of producing functional human tissues and organs.

6.4. Process simulation and optimization

In bioprinting, process simulation and optimization are crucial to ensuring the achievement of minimum feature sizes, printing accuracy, and mechanical properties. Unlike conventional manufacturing processes, bioprinting calls for closer monitoring of the interaction between process parameters and the resulting material properties to ensure the stability of biological components. The inherent complexity and environmental sensitivity of bioink formulations bring additional challenges to the development of high-fidelity computer simulation and optimization routines, especially for heterogeneous material deposition. Since concurrent process simulation models and approaches are limited in their scope, scale, and accuracy, substantial research efforts are required to accelerate the clinical translation of bioprinting. In the future, tools from machine learning or deep learning will have to be adapted to predict better the effect of process parameters on the resulting biological constructs. Additionally, the integration of real-time simulation and feedback loop control in additive manufacturing systems is critical in achieving controllable fabrication performances.

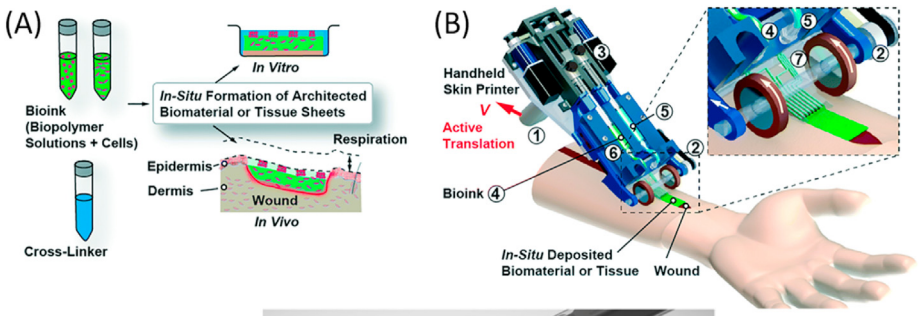

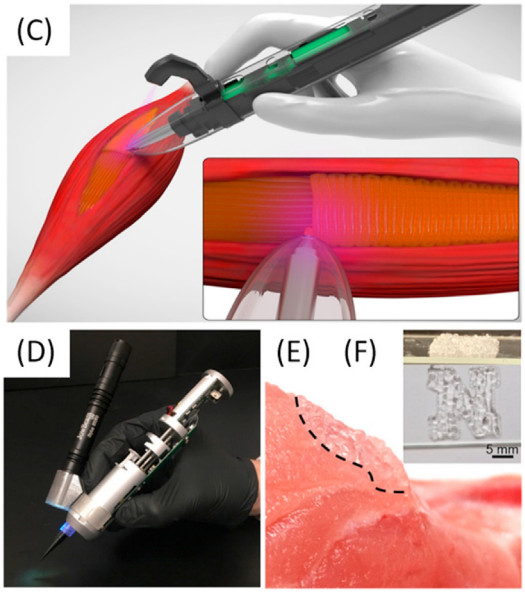

Fig. 12. (A–B) Schematic diagram showing the working principle and design of a handheld skin printer developed by Hakimi and co-workers. Reproduced with permission from Ref. [142], Copyright 2018, Royal Society of Chemistry. (C–F) Tamayol et al. demonstrated the *in situ* bioprinting of GelMA scaffolds for treating VML injuries. They demonstrated the printing of a typical scaffold on non-planar porcine skeletal muscle. Reproduced with permission from Ref. [23], Copyright 2020, ACS Publications.

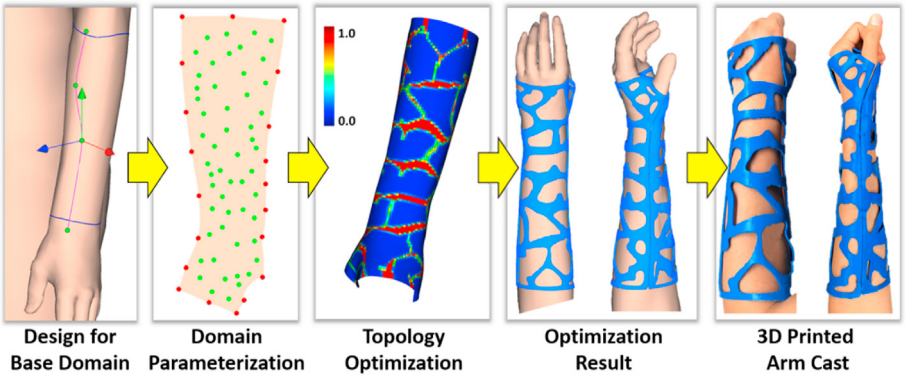

Fig. 13. A computational tool developed by Zhang et al. for designing and optimizing a customized arm cast. The tool was built upon signed distance field and topology optimization. Reproduced with permission from Ref. [148], Copyright 2019, Elsevier.

6.5. *Inspection and quality control*

For widespread clinical adaptation of bioprinting, inspection, and quality control tools will have to be instituted for identifying, mitigating and correcting defects (biological, structural, and dimensional). Quality assurance of bioprinted constructs encompasses both geometric integrity and biological functions [149]. High-precision 3D scanners augmented with verified computational algorithms and tools from computer vision remain to be adapted to acquire and evaluate the geometric variation between the printed organs and the computer-designed 3D models. The complexity of the inspection process is compounded by the fact that most of the bioprinted constructs are usually freeform shapes, thus, requiring detailed error evaluation.

Surface scanning of bioprinted scaffolds containing heterogeneous materials and biological molecules will not be sufficient. Instead, volumetric scanning using CT or MRI systems will have to be utilized for defect identification and evaluation. Although the dimensional accuracy of printed structures can be quantified using fast and relatively accurate geometric modeling algorithms, assessing biological functionality remains a formidable challenge. Therefore, non-destructive evaluation of biological functionality is a key consideration. A feasible solution would be to utilize the geometric and material information obtained from volumetric scans to simulate the functionality of the organs, which will necessitate the establishment of their relationships with the biological functions of the printed constructs. In this regard, machine learning or deep learning-based methods could potentially be adapted to define these relationships.

7. Conclusions

This review provides a broad overview of ongoing research in EBB and specifically focuses on the importance of rheological properties and process parameters that have a consequential influence on the printability of bioinks. Currently, there is a large body of work driving advancements in directions such as bioink formulations, higher resolution printing, and complete automation. However, for mainstream clinical adaption of EBB, we identify the following avenues for future research: (1) standardized protocols for the development and screening of bioinks, (2) real-time in-process sensing, monitoring, fault diagnosis, and control, (3) high-throughput production, and quality assurance of bioprinted constructs through novel in-situ and ex-situ modalities, and (4) fundamental process models to predict the effect of process parameters, construct shape and features, and materials properties on the quality (geometry and biological functionality) of the construct. We forsee, as in other additive manufacturing technologies, that incorporation of tools from machine learning and deep learning will likely play a key role in ensuring the quality of bioprinted construsts.

Declaration of competing interest

The authors declare that they have no known competing financial interests or personal relationships that could have appeared to influence the work reported in this paper.

Acknowledgements

The concept of in-situ imaging for process monitoring and assessing the effect of process conditions on the quality of 3D printed biomaterial deposits was funded through CMMI-1739696 (Program Officer: Dr. Bruce Kramer).

References

[1] R. Langer, J.P. Vacanti, Tissue engineering, Science 80 (1993), https://doi.org/10.1126/science.8493529.
[2] J.P. Vacanti, R. Langer, Tissue engineering: the design and fabrication of living replacement devices for surgical reconstruction and transplantation, Lancet (1999), https://doi.org/10.1016/s0140-6736(99)90247-7.
[3] F.J. O'Brien, Biomaterials & scaffolds for tissue engineering, Mater. Today (2011), https://doi.org/10.1016/S1369-7021(11)70058-X.
[4] A. Tamayol, M. Akbari, N. Annabi, A. Paul, A. Khademhosseini, D. Juncker, Fiber-based tissue engineering: progress, challenges, and opportunities, Biotechnol. Adv. (2013), https://doi.org/10.1016/j.biotechadv.2012.11.007.
[5] B. Dhandayuthapani, Y. Yoshida, T. Maekawa, D.S. Kumar, Polymeric scaffolds in tissue engineering application: a review, Int. J. Polym. Sci. (2011), https://doi.org/10.1155/2011/290602.
[6] K. Elkhoury, C.S. Russell, L. Sanchez-Gonzalez, A. Mostafavi, T.J. Williams, C. Kahn, N.A. Peppas, E. Arab-Tehrany, A. Tamayol, Soft-nanoparticle functionalization of natural hydrogels for tissue engineering applications, Adv. Healthc. Mater. (2019), https://doi.org/10.1002/adhm.201900506.
[7] S. Ramesh, L. Lungaro, D. Tsikritsis, E. Weflen, I.V. Rivero, A.P.D. Elfick, Fabrication and evaluation of poly(lactic acid), chitosan, and tricalcium phosphate biocomposites for guided bone regeneration, J. Appl. Polym. Sci. (2018), https://doi.org/10.1002/app.46692.
[8] E. Carletti, A. Motta, C. Migliaresi, Scaffolds for tissue engineering and 3D cell culture, Methods Mol. Biol. (2011), https://doi.org/10.1007/978-1-60761-984-0_2.
[9] V.L. Tsang, S.N. Bhatia, Fabrication of three-dimensional tissues, Adv. Biochem. Eng. Biotechnol. (2006), https://doi.org/10.1007/10_010.
[10] H.W. Kang, D.W. Cho, Development of an indirect stereolithography technology for scaffold fabrication with a wide range of biomaterial selectivity, Tissue Eng. C Methods (2012), https://doi.org/10.1089/ten.tec.2011.0621.
[11] Y. Zhang, H. Ouyang, T.L. Chwee, S. Ramakrishna, Z.M. Huang, Electrospinning of gelatin fibers and gelatin/PCL composite fibrous scaffolds, J. Biomed. Mater. Res. B Appl. Biomater. (2005), https://doi.org/10.1002/jbm.b.30128.
[12] L. Shor, S. Güçeri, X. Wen, M. Gandhi, W. Sun, Fabrication of three-dimensional polycaprolactone/hydroxyapatite tissue scaffolds and osteoblast-scaffold interactions in vitro, Biomaterials (2007), https://doi.org/10.1016/j.biomaterials.2007.08.018.
[13] A. Tamayol, A.H. Najafabadi, B. Aliakbarian, E. Arab-Tehrany, M. Akbari, N. Annabi, D. Juncker, A. Khademhosseini, Hydrogel templates for rapid manufacturing of bioactive fibers and 3D constructs, Adv. Healthc. Mater. (2015), https://doi.org/10.1002/adhm.201500492.
[14] A. Fallahi, I.K. Yazdi, L. Serex, E. Lesha, N. Faramarzi, F. Tarlan, H. Avci, R. Costa-Almeida, F. Sharifi, C. Rinoldi, M.E. Gomes, S.R. Shin, A. Khademhosseini, M. Akbari, A. Tamayol, Customizable composite fibers for engineering skeletal muscle models, ACS Biomater. Sci. Eng. (2020), https://doi.org/10.1021/acsbiomaterials.9b00992.
[15] W. Gao, Y. Zhang, D. Ramanujan, K. Ramani, Y. Chen, C.B. Williams, C.C.L. Wang, Y.C. Shin, S. Zhang, P.D. Zavattieri, The status, challenges, and future of additive manufacturing in engineering, CAD Comput. Aided Des (2015), https://doi.org/10.1016/j.cad.2015.04.001.
[16] E. Desimone, K. Schacht, T. Jungst, J. Groll, T. Scheibel, Biofabrication of 3D constructs: fabrication technologies and spider silk proteins as bioinks, Pure Appl. Chem. (2015), https://doi.org/10.1515/pac-2015-0106.
[17] A. Farzin, A.K. Miri, F. Sharifi, N. Faramarzi, A. Jaberi, A. Mostafavi, R. Solorzano, Y.S. Zhang, N. Annabi, A. Khademhosseini, A. Tamayol, 3D-Printed sugar-based stents facilitating vascular anastomosis, Adv. Healthc. Mater. (2018), https://doi.org/10.1002/adhm.201800702.
[18] N. Faramarzi, I.K. Yazdi, M. Nabavinia, A. Gemma, A. Fanelli, A. Caizzone, L.M. Ptaszek, I. Sinha, A. Khademhosseini, J.N. Ruskin, A. Tamayol, Patient-specific bioinks for 3D bioprinting of tissue engineering scaffolds, Adv. Healthc. Mater. (2018), https://doi.org/10.1002/adhm.201701347.
[19] I.T. Ozbolat, Y. Yu, Bioprinting toward organ fabrication: challenges and future trends, IEEE Trans. Biomed. Eng. (2013), https://doi.org/10.1109/TBME.2013.2243912.
[20] A.V. Do, B. Khorsand, S.M. Geary, A.K. Salem, 3D printing of scaffolds for tissue regeneration applications, Adv. Healthc. Mater. (2015), https://doi.org/10.1002/adhm.201500168.
[21] A.B. Dababneh, I.T. Ozbolat, Bioprinting Technology, A current state-of-the-art review, J. Manuf. Sci. Eng. (2014), https://doi.org/10.1115/1.4028512.
[22] S. V Murphy, A. Atala, 3D bioprinting of tissues and organs, Nat. Biotechnol. 32 (2014) 773–785, https://doi.org/10.1038/nbt.2958.
[23] C.S. Russell, A. Mostafavi, J.P. Quint, A.C. Panayi, K. Baldino, T.J. Williams, J.G. Daubendiek, V. Hugo Sánchez, Z. Bonick, M. Trujillo-Miranda, S.R. Shin, O. Pourquie, S. Salehi, I. Sinha, A. Tamayol, In situ printing of adhesive hydrogel scaffolds for the treatment of skeletal muscle injuries, ACS Appl. Bio Mater. (2020), https://doi.org/10.1021/acsabm.9b01176.
[24] I.T. Ozbolat, M. Hospodiuk, Current advances and future perspectives in extrusion-based bioprinting, Biomaterials (2016), https://doi.org/10.1016/j.biomaterials.2015.10.076.
[25] M. Kesti, M. Müller, J. Becher, M. Schnabelrauch, M. D'Este, D. Eglin, M. Zenobi-Wong, A versatile bioink for three-dimensional printing of cellular scaffolds based on thermally and photo-triggered tandem gelation, Acta Biomater. (2015), https://doi.org/10.1016/j.actbio.2014.09.033.
[26] G. Gillispie, P. Prim, J. Copus, J. Fisher, A.G. Mikos, J.J. Yoo, A. Atala, S.J. Lee, Assessment methodologies for extrusion-based bioink printability, Biofabrication (2020), https://doi.org/10.1088/1758-5090/ab6f0d.
[27] K. Hölzl, S. Lin, L. Tytgat, S. Van Vlierberghe, L. Gu, A. Ovsianikov, Bioink properties before, during and after 3D bioprinting, Biofabrication (2016), https://doi.org/10.1088/1758-5090/8/3/032002.
[28] M. Müller, J. Becher, M. Schnabelrauch, M. Zenobi-Wong, Nanostructured Pluronic hydrogels as bioinks for 3D bioprinting, Biofabrication (2015), https://doi.org/10.1088/1758-5090/7/3/035006.
[29] D. Wu, Y. Yu, J. Tan, L. Huang, B. Luo, L. Lu, C. Zhou, 3D bioprinting of gellan gum and poly (ethylene glycol) diacrylate based hydrogels to produce human-scale constructs with high-fidelity, Mater. Des. (2018), https://doi.org/10.1016/j.matdes.2018.09.040.
[30] S. Ghorbanian, M.A. Qasaimeh, M. Akbari, A. Tamayol, D. Juncker, Microfluidic direct writer with integrated declogging mechanism for fabricating cell-laden hydrogel constructs, Biomed. Microdevices (2014), https://doi.org/10.1007/s10544-014-9842-8.
[31] W. Lee, J.C. Debasitis, V.K. Lee, J.H. Lee, K. Fischer, K. Edminster, J.K. Park, S.S. Yoo, Multi-layered culture of human skin fibroblasts and keratinocytes through three-dimensional freeform fabrication, Biomaterials (2009), https://doi.org/10.1016/j.biomaterials.2008.12.009.
[32] B. Byambaa, N. Annabi, K. Yue, G. Trujillo-de Santiago, M.M. Alvarez, W. Jia, M. Kazemzadeh-Narbat, S.R. Shin, A. Tamayol, A. Khademhosseini, Bioprinted osteogenic and vasculogenic patterns for engineering 3D bone tissue, Adv. Healthc. Mater. (2017), https://doi.org/10.1002/adhm.201700015.
[33] D.F. Duarte Campos, A. Blaeser, A. Korsten, S. Neuss, J. Jäkel, M. Vogt, H. Fischer, The stiffness and structure of three-dimensional printed hydrogels direct the differentiation of mesenchymal stromal cells toward adipogenic and osteogenic lineages, Tissue Eng. 21 (2015) 740–756, https://doi.org/10.1089/ten.tea.2014.0231.
[34] D.B. Kolesky, K.A. Homan, M.A. Skylar-Scott, J.A. Lewis, Three-dimensional bioprinting of thick vascularized tissues, Proc. Natl. Acad. Sci. U. S. A. (2016), https://doi.org/10.1073/pnas.1521342113.
[35] X. Ma, C. Yu, P. Wang, W. Xu, X. Wan, C.S.E. Lai, J. Liu, A. Koroleva-Maharajh, S. Chen, Rapid 3D bioprinting of decellularized extracellular matrix with regionally varied mechanical properties and biomimetic microarchitecture, Biomaterials (2018), https://doi.org/10.1016/j.biomaterials.2018.09.026.
[36] W. Jia, P.S. Gungor-Ozkerim, Y.S. Zhang, K. Yue, K. Zhu, W. Liu, Q. Pi, B. Byambaa, M.R. Dokmeci, S.R. Shin, A. Khademhosseini, Direct 3D bioprinting of perfusable vascular constructs using a blend bioink, Biomaterials (2016), https://doi.org/10.1016/j.biomaterials.2016.07.038.
[37] Y. Yu, K.K. Moncal, J. Li, W. Peng, I. Rivero, J.A. Martin, I.T. Ozbolat, Three-dimensional bioprinting using self-Assembling scalable scaffold-free "tissue strands" as a new bioink, Sci. Rep. (2016), https://doi.org/10.1038/srep28714.

[38] S. Wüst, M.E. Godla, R. Müller, S. Hofmann, Tunable hydrogel composite with two-step processing in combination with innovative hardware upgrade for cell-based three-dimensional bioprinting, Acta Biomater. (2014), https://doi.org/10.1016/j.actbio.2013.10.016.

[39] L.E. Bertassoni, M. Cecconi, V. Manoharan, M. Nikkhah, J. Hjortnaes, A.L. Cristino, G. Barabaschi, D. Demarchi, M.R. Dokmeci, Y. Yang, A. Khademhosseini, Hydrogel bioprinted microchannel networks for vascularization of tissue engineering constructs, Lab Chip (2014), https://doi.org/10.1039/c4lc00030g.

[40] L. Ouyang, R. Yao, Y. Zhao, W. Sun, Effect of bioink properties on printability and cell viability for 3D bioplotting of embryonic stem cells, Biofabrication (2016), https://doi.org/10.1088/1758-5090/8/3/035020.

[41] N. Paxton, W. Smolan, T. Böck, F. Melchels, J. Groll, T. Jungst, Proposal to assess printability of bioinks for extrusion-based bioprinting and evaluation of rheological properties governing bioprintability, Biofabrication (2017), https://doi.org/10.1088/1758-5090/aa8dd8.

[42] L. Shi, H. Carstensen, K. Hölzl, M. Lunzer, H. Li, J. Hilborn, A. Ovsianikov, D.A. Ossipov, Dynamic coordination Chemistry enables free directional printing of biopolymer hydrogel, Chem. Mater. (2017), https://doi.org/10.1021/acs.chemmater.7b00128.

[43] A. Ribeiro, M.M. Blokzijl, R. Levato, C.W. Visser, M. Castilho, W.E. Hennink, T. Vermonden, J. Malda, Assessing bioink shape fidelity to aid material development in 3D bioprinting, Biofabrication (2018), https://doi.org/10.1088/1758-5090/aa90e2.

[44] A.L. Rutz, P.L. Lewis, R.N. Shah, Toward next-generation bioinks: tuning material properties pre- and post-printing to optimize cell viability, MRS Bull. (2017), https://doi.org/10.1557/mrs.2017.162.

[45] R.F. Pereira, A. Sousa, C.C. Barrias, P.J. Bártolo, P.L. Granja, A single-component hydrogel bioink for bioprinting of bioengineered 3D constructs for dermal tissue engineering, Mater. Horizons. (2018), https://doi.org/10.1039/c8mh00525g.

[46] J. Groll, T. Boland, T. Blunk, J.A. Burdick, D.W. Cho, P.D. Dalton, B. Derby, G. Forgacs, Q. Li, V.A. Mironov, L. Moroni, M. Nakamura, W. Shu, S. Takeuchi, G. Vozzi, T.B.F. Woodfield, T. Xu, J.J. Yoo, J. Malda, Biofabrication, Reappraising the definition of an evolving field, Biofabrication (2016), https://doi.org/10.1088/1758-5090/8/1/013001.

[47] A.M. Holmes, A. Charlton, B. Derby, L. Ewart, A. Scott, W. Shu, Rising to the challenge: applying biofabrication approaches for better drug and chemical product development, Biofabrication (2017), https://doi.org/10.1088/1758-5090/aa7bbd.

[48] G. Skeldon, B. Lucendo-Villarin, W. Shu, Three-dimensional bioprinting of stem-cell derived tissues for human regenerative medicine, Philos. Trans. R. Soc. B Biol. Sci. (2018), https://doi.org/10.1098/rstb.2017.0224.

[49] B.H. Lee, N. Lum, L.Y. Seow, P.Q. Lim, L.P. Tan, Synthesis and characterization of types A and B gelatin methacryloyl for bioink applications, Materials 9 (2016) 1–13, https://doi.org/10.3390/ma9100797.

[50] D.Y. Lee, H. Lee, Y. Kim, S.Y. Yoo, W.J. Chung, G. Kim, Phage as versatile nanoink for printing 3-D cell-laden scaffolds, Acta Biomater. (2016), https://doi.org/10.1016/j.actbio.2015.10.004.

[51] C. Norotte, F.S. Marga, L.E. Niklason, G. Forgacs, Scaffold-free vascular tissue engineering using bioprinting, Biomaterials (2009), https://doi.org/10.1016/j.biomaterials.2009.06.034.

[52] T. Ahlfeld, G. Cidonio, D. Kilian, S. Duin, A.R. Akkineni, J.I. Dawson, S. Yang, A. Lode, R.O.C. Oreffo, M. Gelinsky, Development of a clay based bioink for 3D cell printing for skeletal application, Biofabrication (2017), https://doi.org/10.1088/1758-5090/aa7e96.

[53] R. Levato, J. Visser, J.A. Planell, E. Engel, J. Malda, M.A. Mateos-Timoneda, Biofabrication of tissue constructs by 3D bioprinting of cell-laden microcarriers, Biofabrication (2014), https://doi.org/10.1088/1758-5082/6/3/035020.

[54] K. Schacht, T. Jüngst, M. Schweinlin, A. Ewald, J. Groll, T. Scheibel, Biofabrication of cell-loaded 3D spider silk constructs, Angew. Chem. Int. Ed. (2015), https://doi.org/10.1002/anie.201409846.

[55] J. Malda, J. Visser, F.P. Melchels, T. Jüngst, W.E. Hennink, W.J.A. Dhert, J. Groll, D.W. Hutmacher, 25th anniversary article: engineering hydrogels for biofabrication, Adv. Mater. (2013), https://doi.org/10.1002/adma.201302042.

[56] S. AnilKumar, S.C. Allen, N. Tasnim, T. Akter, S. Park, A. Kumar, M. Chattopadhyay, Y. Ito, L.J. Suggs, B. Joddar, The applicability of furfuryl-gelatin as a novel bioink for tissue engineering applications, J. Biomed. Mater. Res. B Appl. Biomater. (2019), https://doi.org/10.1002/jbm.b.34123.

[57] A. Panwar, L.P. Tan, Current status of bioinks for micro-extrusion-based 3D bioprinting, Molecules (2016), https://doi.org/10.3390/molecules21060685.

[58] S. Derakhshanfar, R. Mbeleck, K. Xu, X. Zhang, W. Zhong, M. Xing, 3D bioprinting for biomedical devices and tissue engineering: a review of recent trends and advances, Bioact. Mater. (2018), https://doi.org/10.1016/j.bioactmat.2017.11.008.

[59] J. Park, S.J. Lee, H. Lee, S.A. Park, J.Y. Lee, Three dimensional cell printing with sulfated alginate for improved bone morphogenetic protein-2 delivery and osteogenesis in bone tissue engineering, Carbohydr. Polym. (2018), https://doi.org/10.1016/j.carbpol.2018.05.048.

[60] M.G. Yeo, G.H. Kim, A cell-printing approach for obtaining hASC-laden scaffolds by using a collagen/polyphenol bioink, Biofabrication (2017), https://doi.org/10.1088/1758-5090/aa6997.

[61] S.A. Wilson, L.M. Cross, C.W. Peak, A.K. Gaharwar, Shear-thinning and thermo-reversible nanoengineered inks for 3D bioprinting, ACS Appl. Mater. Interfaces (2017), https://doi.org/10.1021/acsami.7b13602.

[62] J. Gopinathan, I. Noh, Recent trends in bioinks for 3D printing, Biomater. Res. (2018), https://doi.org/10.1186/s40824-018-0122-1.

[63] J. Jia, D.J. Richards, S. Pollard, Y. Tan, J. Rodriguez, R.P. Visconti, T.C. Trusk, M.J. Yost, H. Yao, R.R. Markwald, Y. Mei, Engineering alginate as bioink for bioprinting, Acta Biomater. (2014), https://doi.org/10.1016/j.actbio.2014.06.034.

[64] G. Ahn, K.H. Min, C. Kim, J.S. Lee, D. Kang, J.Y. Won, D.W. Cho, J.Y. Kim, S. Jin, W.S. Yun, J.H. Shim, Precise stacking of decellularized extracellular matrix based 3D cell-laden constructs by a 3D cell printing system equipped with heating modules, Sci. Rep. 7 (2017) 1–11, https://doi.org/10.1038/s41598-017-09201-5.

[65] J. Göhl, K. Markstedt, A. Mark, K. Håkansson, P. Gatenholm, F. Edelvik, Simulations of 3D bioprinting: predicting bioprintability of nanofibrillar inks, Biofabrication 10 (2018) 34105, https://doi.org/10.1088/1758-5090/aac872.

[66] Y. Chen, Y. Wang, Q. Yang, Y. Liao, B. Zhu, G. Zhao, R. Shen, X. Lu, S. Qu, A novel thixotropic magnesium phosphate-based bioink with excellent printability for application in 3D printing, J. Mater. Chem. B. 6 (2018) 4502–4513, https://doi.org/10.1039/c8tb01196f.

[67] Z. Li, S. Huang, Y. Liu, B. Yao, T. Hu, H. Shi, J. Xie, X. Fu, Tuning alginate-gelatin bioink properties by varying solvent and their impact on stem cell behavior, Sci. Rep. 8 (2018) 1–8, https://doi.org/10.1038/s41598-018-26407-3.

[68] S. Midha, S. Ghosh, Silk-based bioinks for 3D bioprinting, Regen. Med. Lab. to Clin. 1701204 (2017) 259–276, https://doi.org/10.1007/978-981-10-3701-6_15.

[69] C.D. Andrew, E.C. Susan, M.R. Emily, J.K. Daniel, A comparison of different bioinks for 3D bioprinting of fibrocartilage and hyaline cartilage, Biofabrication 8 (2016) 45002. http://stacks.iop.org/1758-5090/8/i=4/a=045002.

[70] D. Petta, A.R. Armiento, D. Grijpma, M. Alini, D. Eglin, M. D'Este, 3D bioprinting of a hyaluronan bioink through enzymatic-and visible light-crosslinking, Biofabrication 10 (2018), https://doi.org/10.1088/1758-5090/aadf58.

[71] Y. Loo, A. Lakshmanan, M. Ni, L.L. Toh, S. Wang, C.A.E. Hauser, Peptide bioink: self-assembling nanofibrous scaffolds for three-dimensional organotypic cultures, Nano Lett. (2015), https://doi.org/10.1021/acs.nanolett.5b02859.

[72] Y.W. Koo, E.J. Choi, J.Y. Lee, H.J. Kim, G.H. Kim, S.H. Do, 3D printed cell-laden collagen and hybrid scaffolds for in vivo articular cartilage tissue regeneration, J. Ind. Eng. Chem. 66 (2018) 343–355, https://doi.org/10.1016/j.jiec.2018.05.049.

[73] J. Lee, C.H. Park, C.S. Kim, Microcylinder-laden gelatin-based bioink engineered for 3D bioprinting, Mater. Lett. (2018), https://doi.org/10.1016/j.matlet.2018.08.138.

[74] M. Müller, E. Öztürk, Ø. Arlov, P. Gatenholm, M. Zenobi-Wong, Alginate sulfate–nanocellulose bioinks for cartilage bioprinting applications, Ann. Biomed. Eng. (2017), https://doi.org/10.1007/s10439-016-1704-5.

[75] F.E. Freeman, D.J. Kelly, Tuning alginate bioink stiffness and composition for controlled growth factor delivery and to spatially direct MSC Fate within bioprinted tissues, Sci. Rep. 7 (2017) 1–12, https://doi.org/10.1038/s41598-017-17286-1.

[76] M. Hospodiuk, M. Dey, D. Sosnoski, I.T. Ozbolat, The bioink: a comprehensive review on bioprintable materials, Biotechnol. Adv. (2017), https://doi.org/10.1016/j.biotechadv.2016.12.006.

[77] A. Athirasala, A. Tahayeri, G. Thrivikraman, C.M. Franca, N. Monteiro, V. Tran, J. Ferracane, L.E. Bertassoni, A dentin-derived hydrogel bioink for 3D bioprinting of cell laden scaffolds for regenerative dentistry, Biofabrication 10 (2018), https://doi.org/10.1088/1758-5090/aa9b4e.

[78] J.H.Y. Chung, S. Naficy, Z. Yue, R. Kapsa, A. Quigley, S.E. Moulton, G.G. Wallace, Bio-ink properties and printability for extrusion printing living cells, Biomater. Sci. (2013), https://doi.org/10.1039/c3bm00012e.

[79] A. Abbadessa, M.M. Blokzijl, V.H.M. Mouser, P. Marica, J. Malda, W.E. Hennink, T. Vermonden, A thermo-responsive and photo-polymerizable chondroitin sulfate-based hydrogel for 3D printing applications, Carbohydr. Polym. (2016), https://doi.org/10.1016/j.carbpol.2016.04.080.

[80] J.H. Kim, J.J. Yoo, S.J. Lee, Three-dimensional cell-based bioprinting for soft tissue regeneration, Tissue Eng. Regen. Med (2016), https://doi.org/10.1007/s13770-016-0133-8.

[81] G.R. López-Marcial, A.Y. Zeng, C. Osuna, J. Dennis, J.M. García, G.D. O'Connell, Agarose-based hydrogels as suitable bioprinting materials for tissue engineering, ACS Biomater. Sci. Eng. 4 (2018) 3610–3616, https://doi.org/10.1021/acsbiomaterials.8b00903.

[82] H. Li, S. Liu, L. Lin, Rheological study on 3D printability of alginate hydrogel and effect of graphene oxide, Int. J. Bioprinting. (2016), https://doi.org/10.18063/IJB.2016.02.007.

[83] V. Mironov, T. Boland, T. Trusk, G. Forgacs, R.R. Markwald, Organ printing: computer-aided jet-based 3D tissue engineering, Trends Biotechnol. (2003), https://doi.org/10.1016/S0167-7799(03)00033-7.

[84] S. Khalil, J. Nam, W. Sun, Multi-nozzle deposition for construction of 3D biopolymer tissue scaffolds, Rapid Prototyp. J. (2005), https://doi.org/10.1108/13552540510573347.

[85] F. Momen-Heravi, L. Balaj, S. Alian, A.J. Trachtenberg, F.H. Hochberg, J. Skog, W.P. Kuo, Impact of biofluid viscosity on size and sedimentation efficiency of the isolated microvesicles, Front. Physiol. (2012), https://doi.org/10.3389/fphys.2012.00162.

[86] A.G. Tabriz, M.A. Hermida, N.R. Leslie, W. Shu, Three-dimensional bioprinting of complex cell laden alginate hydrogel structures, Biofabrication (2015), https://doi.org/10.1088/1758-5090/7/4/045012.

[87] B.A. Aguado, W. Mulyasasmita, J. Su, K.J. Lampe, S.C. Heilshorn, Improving viability of stem cells during syringe needle flow through the design of hydrogel cell carriers, Tissue Eng. (2012), https://doi.org/10.1089/ten.tea.2011.0391.

[88] J. Jang, T.G. Kim, B.S. Kim, S.W. Kim, S.M. Kwon, D.W. Cho, Tailoring mechanical properties of decellularized extracellular matrix bioink by vitamin B2-induced

photo-crosslinking, Acta Biomater. (2016), https://doi.org/10.1016/j.actbio.2016.01.013.
[89] H. Li, Y.J. Tan, S. Liu, L. Li, Three-dimensional bioprinting of oppositely charged hydrogels with super strong interface bonding, ACS Appl. Mater. Interfaces 10 (2018) 11164–11174, https://doi.org/10.1021/acsami.7b19730.
[90] IUPAC compendium of chemical terminology, Choice Rev. Online. (2003), https://doi.org/10.5860/choice.40sup-0262.
[91] S. Ramesh, V. Kovelakuntla, A.S. Meyer, I.V. Rivero, Three-dimensional printing of stimuli-responsive hydrogel with antibacterial activity, Bioprinting (2020), https://doi.org/10.1016/j.bprint.2020.e00106.
[92] M.H. Kim, Y.W. Lee, W.K. Jung, J. Oh, S.Y. Nam, Enhanced rheological behaviors of alginate hydrogels with carrageenan for extrusion-based bioprinting, J. Mech. Behav. Biomed. Mater. (2019), https://doi.org/10.1016/j.jmbbm.2019.06.014.
[93] C.R. Alcala-Orozco, I. Mutreja, X. Cui, D. Kumar, G.J. Hooper, K.S. Lim, T.B.F. Woodfield, Design and characterisation of multi-functional strontium-gelatin nanocomposite bioinks with improved print fidelity and osteogenic capacity, Bioprinting (2020), https://doi.org/10.1016/j.bprint.2019.e00073.
[94] K. Markstedt, A. Mantas, I. Tournier, H. Martínez Ávila, D. Hägg, P. Gatenholm, 3D bioprinting human chondrocytes with nanocellulose-alginate bioink for cartilage tissue engineering applications, Biomacromolecules (2015), https://doi.org/10.1021/acs.biomac.5b00188.
[95] S. Shin, S. Park, M. Park, E. Jeong, K. Na, H.J. Youn, J. Hyun, Cellulose nanofibers for the enhancement of printability of low viscosity gelatin derivatives, BioResources (2017), https://doi.org/10.15376/biores.12.2.2941-2954.
[96] A. Sheikhi, S. Afewerki, R. Oklu, A.K. Gaharwar, A. Khademhosseini, Effect of ionic strength on shear-thinning nanoclay-polymer composite hydrogels, Biomater. Sci. (2018), https://doi.org/10.1039/c8bm00469b.
[97] Y. Jin, W. Chai, Y. Huang, Printability study of hydrogel solution extrusion in nanoclay yield-stress bath during printing-then-gelation biofabrication, Mater. Sci. Eng. C (2017), https://doi.org/10.1016/j.msec.2017.05.144.
[98] C.B. Highley, C.B. Rodell, J.A. Burdick, Direct 3D printing of shear-thinning hydrogels into self-healing hydrogels, Adv. Mater. (2015), https://doi.org/10.1002/adma.201501234.
[99] J. Malda, J. Visser, F.P. Melchels, T. Jüngst, W.E. Hennink, W.J.A. Dhert, J. Groll, D.W. Hutmacher, 25th anniversary article: engineering hydrogels for biofabrication, Adv. Mater. (2013), https://doi.org/10.1002/adma.201302042.
[100] E.A. Kiyotake, A.W. Douglas, E.E. Thomas, S.L. Nimmo, M.S. Detamore, Development and quantitative characterization of the precursor rheology of hyaluronic acid hydrogels for bioprinting, Acta Biomater. (2019), https://doi.org/10.1016/j.actbio.2019.01.041.
[101] V.H.M. Mouser, F.P.W. Melchels, J. Visser, W.J.A. Dhert, D. Gawlitta, J. Malda, Yield stress determines bioprintability of hydrogels based on gelatin-methacryloyl and gellan gum for cartilage bioprinting, Biofabrication (2016), https://doi.org/10.1088/1758-5090/8/3/035003.
[102] K. Nair, M. Gandhi, S. Khalil, K.C. Yan, M. Marcolongo, K. Barbee, W. Sun, Characterization of cell viability during bioprinting processes, Biotechnol. J. (2009), https://doi.org/10.1002/biot.200900004.
[103] N. Diamantides, L. Wang, T. Pruiksma, J. Siemiatkoski, C. Dugopolski, S. Shortkroff, S. Kennedy, L.J. Bonassar, Correlating rheological properties and printability of collagen bioinks: the effects of riboflavin photocrosslinking and pH, Biofabrication (2017), https://doi.org/10.1088/1758-5090/aa780f.
[104] Y. Zhao, Y. Li, S. Mao, W. Sun, R. Yao, The influence of printing parameters on cell survival rate and printability in microextrusion-based 3D cell printing technology, Biofabrication (2015), https://doi.org/10.1088/1758-5090/7/4/045002.
[105] T. Gao, G.J. Gillispie, J.S. Copus, A.K. Pr, Y. Seol, Optimization of gelatin – alginate composite bioink printability using rheological parameters : a systematic approach Optimization of gelatin – alginate composite bioink printability using rheological parameters : a systematic approach, (n.d.). https://doi.org/10.1088.
[106] B.H. Lee, N. Lum, L.Y. Seow, P.Q. Lim, L.P. Tan, Synthesis and characterization of types A and B gelatin methacryloyl for bioink applications, Materials (Basel). https://doi.org/10.3390/ma9100797, 2016.
[107] W.L. Ng, W.Y. Yeong, M.W. Naing, Polyelectrolyte gelatin-chitosan hydrogel optimized for 3D bioprinting in skin tissue engineering, Int. J. Bioprinting (2016), https://doi.org/10.18063/ijb.2016.01.009.
[108] A. Blaeser, D.F. Duarte Campos, U. Puster, W. Richtering, M.M. Stevens, H. Fischer, Controlling shear stress in 3D bioprinting is a key factor to balance printing resolution and stem cell integrity, Adv. Healthc. Mater. (2016), https://doi.org/10.1002/adhm.201500677.
[109] T. Billiet, E. Gevaert, T. De Schryver, M. Cornelissen, P. Dubruel, The 3D printing of gelatin methacrylamide cell-laden tissue-engineered constructs with high cell viability, Biomaterials (2014), https://doi.org/10.1016/j.biomaterials.2013.09.078.
[110] M. Müller, E. Öztürk, Ø. Arlov, P. Gatenholm, M. Zenobi-Wong, Alginate sulfate–nanocellulose bioinks for cartilage bioprinting applications, Ann. Biomed. Eng. 45 (2017) 210–223, https://doi.org/10.1007/s10439-016-1704-5.
[111] B. Webb, B.J. Doyle, Parameter optimization for 3D bioprinting of hydrogels, Bioprinting (2017), https://doi.org/10.1016/j.bprint.2017.09.001.
[112] T.Q. Trung, N.E. Lee, Flexible and stretchable physical sensor integrated platforms for wearable human-activity monitoringand personal healthcare, Adv. Mater. (2016), https://doi.org/10.1002/adma.201504244.
[113] G.R. López-Marcial, A.Y. Zeng, C. Osuna, J. Dennis, J.M. García, G.D. O'Connell, Agarose-based hydrogels as suitable bioprinting materials for tissue engineering, ACS Biomater. Sci. Eng. (2018), https://doi.org/10.1021/acsbiomaterials.8b00903.
[114] T. Gao, G.J. Gillispie, J.S. Copus, A.P.R. Kumar, Y.J. Seol, A. Atala, J.J. Yoo, S.J. Lee, Optimization of gelatin-alginate composite bioink printability using rheological parameters: a systematic approach, Biofabrication (2018), https://doi.org/10.1088/1758-5090/aacdc7.
[115] I.P. Magalhães, P.M. de Oliveira, J. Dernowsek, E.B. Las Casas, M.S. Las Casas, Nvestigation of the effect of nozzle design on rheological bioprinting properties using computational fluid dynamics. I, 2019, https://doi.org/10.1590/s1517-707620190003.0714. Matéria (Rio Janeiro).
[116] S. Knowlton, B. Yenilmez, S. Anand, S. Tasoglu, Photocrosslinking-based bioprinting: examining crosslinking schemes, Bioprinting (2017), https://doi.org/10.1016/j.bprint.2017.03.001.
[117] K. Zhu, S.R. Shin, T. van Kempen, Y.C. Li, V. Ponraj, A. Nasajpour, S. Mandla, N. Hu, X. Liu, J. Leijten, Y.D. Lin, M.A. Hussain, Y.S. Zhang, A. Tamayol, A. Khademhosseini, Gold nanocomposite bioink for printing 3D cardiac constructs, Adv. Funct. Mater. (2017), https://doi.org/10.1002/adfm.201605352.
[118] W.E. Hennink, C.F. van Nostrum, Novel crosslinking methods to design hydrogels, Adv. Drug Deliv. Rev. (2012), https://doi.org/10.1016/j.addr.2012.09.009.
[119] C.D. O'Connell, S. Konate, C. Onofrillo, R. Kapsa, C. Baker, S. Duchi, T. Eekel, Z. Yue, S. Beirne, G. Barnsley, C. Di Bella, P.F. Choong, G.G. Wallace, Free-form co-axial bioprinting of a gelatin methacryloyl bio-ink by direct in situ photo-crosslinking during extrusion, Bioprinting (2020), https://doi.org/10.1016/j.bprint.2020.e00087.
[120] J. Warner, P. Soman, W. Zhu, M. Tom, S. Chen, Design and 3D printing of hydrogel scaffolds with fractal geometries, ACS Biomater. Sci. Eng. (2016), https://doi.org/10.1021/acsbiomaterials.6b00140.
[121] S. Huang, B. Yao, J. Xie, X. Fu, 3D bioprinted extracellular matrix mimics facilitate directed differentiation of epithelial progenitors for sweat gland regeneration, Acta Biomater. (2016), https://doi.org/10.1016/j.actbio.2015.12.039.
[122] J.M. Sobral, S.G. Caridade, R.A. Sousa, J.F. Mano, R.L. Reis, Three-dimensional plotted scaffolds with controlled pore size gradients: effect of scaffold geometry on mechanical performance and cell seeding efficiency, Acta Biomater. (2011), https://doi.org/10.1016/j.actbio.2010.11.003.
[123] S.T. Bendtsen, S.P. Quinnell, M. Wei, Development of a novel alginate-polyvinyl alcohol-hydroxyapatite hydrogel for 3D bioprinting bone tissue engineered scaffolds, J. Biomed. Mater. Res. 105 (2017) 1457–1468, https://doi.org/10.1002/jbm.a.36036.
[124] C.S. Jung, B.K. Kim, J. Lee, B.H. Min, S.H. Park, Development of printable natural cartilage matrix bioink for 3D printing of irregular tissue shape, Tissue Eng. Regen. Med. 15 (2018) 155–162, https://doi.org/10.1007/s13770-017-0104-8.
[125] S. Datta, R. Sarkar, V. Vyas, S. Bhutoria, A. Barui, A. Roy Chowdhury, P. Datta, Alginate-honey bioinks with improved cell responses for applications as bioprinted tissue engineered constructs, J. Mater. Res. (2018), https://doi.org/10.1557/jmr.2018.202.
[126] J.-S. Lee, B.S. Kim, D. Seo, J.H. Park, D.-W. Cho, Three-dimensional cell printing of large-volume tissues: application to ear regeneration, Tissue Eng. C Methods 23 (2017) 136–145, https://doi.org/10.1089/ten.tec.2016.0362.
[127] D. Lee, J.P. Park, M.Y. Koh, P. Kim, J. Lee, M. Shin, H. Lee, Chitosan-catechol: a writable bioink under serum culture media, Biomater. Sci. (2018), https://doi.org/10.1039/c8bm00174j.
[128] D. Petta, D.W. Grijpma, M. Alini, D. Eglin, M. D'Este, Three-dimensional printing of a tyramine hyaluronan derivative with double gelation mechanism for independent tuning of shear thinning and postprinting curing, ACS Biomater. Sci. Eng. 4 (2018) 3088–3098, https://doi.org/10.1021/acsbiomaterials.8b00416.
[129] Y. He, F. Yang, H. Zhao, Q. Gao, B. Xia, J. Fu, Research on the printability of hydrogels in 3D bioprinting, Sci. Rep. (2016), https://doi.org/10.1038/srep29977.
[130] N.P. Thien, R.I. Tanner, A new constitutive equation derived from network theory, J. Nonnewton. Fluid Mech. (1977), https://doi.org/10.1016/0377-0257(77)80021-9.
[131] J.U. Brackbill, D.B. Kothe, C. Zemach, A continuum method for modeling surface tension, J. Comput. Phys. (1992), https://doi.org/10.1016/0021-9991(92)90240-Y.
[132] L. Serex, A. Bertsch, P. Renaud, Microfluidics: a new layer of control for extrusion-based 3D printing, Micromachines (2018), https://doi.org/10.3390/mi9020086.
[133] W. Liu, Y.S. Zhang, M.A. Heinrich, F. De Ferrari, H.L. Jang, S.M. Bakht, M.M. Alvarez, J. Yang, Y.C. Li, G. Trujillo-de Santiago, A.K. Miri, K. Zhu, P. Khoshakhlagh, G. Prakash, H. Cheng, X. Guan, Z. Zhong, J. Ju, G.H. Zhu, X. Jin, S.R. Shin, M.R. Dokmeci, A. Khademhosseini, Rapid continuous multimaterial extrusion bioprinting, Adv. Mater. (2017), https://doi.org/10.1002/adma.201604630.
[134] M.A. Skylar-Scott, J. Mueller, C.W. Visser, J.A. Lewis, Voxelated soft matter via multimaterial multinozzle 3D printing, Nature (2019), https://doi.org/10.1038/s41586-019-1736-8.
[135] P.G. Campbell, L.E. Weiss, Tissue engineering with the aid of inkjet printers, Expet Opin. Biol. Ther. (2007), https://doi.org/10.1517/14712598.7.8.1123.
[136] F. Guillemot, A. Souquet, S. Catros, B. Guillotin, J. Lopez, M. Faucon, B. Pippenger, R. Bareille, M. Rémy, S. Bellance, P. Chabassier, J.C. Fricain, J. Amédée, High-throughput laser printing of cells and biomaterials for tissue engineering, Acta Biomater. (2010), https://doi.org/10.1016/j.actbio.2009.09.029.
[137] K.W. Binder, Situ Bioprinting of the Skin, Wake for, Univ. Grad. Sch. Arts Sci., 2011.
[138] M. Albanna, K.W. Binder, S.V. Murphy, J. Kim, S.A. Qasem, W. Zhao, J. Tan, I.B. El-Amin, D.D. Dice, J. Marco, J. Green, T. Xu, A. Skardal, J.H. Holmes, J.D. Jackson, A. Atala, J.J. Yoo, In situ bioprinting of autologous skin cells accelerates wound healing of extensive excisional full-thickness wounds, Sci. Rep. (2019), https://doi.org/10.1038/s41598-018-38366-w.
[139] A. Skardal, D. Mack, E. Kapetanovic, A. Atala, J.D. Jackson, J. Yoo, S. Soker, Bioprinted amniotic fluid-derived stem cells accelerate healing of large skin

wounds, Stem Cells Transl. Med (2012), https://doi.org/10.5966/sctm.2012-0088.
[140] C.D. O'Connell, C. Di Bella, F. Thompson, C. Augustine, S. Beirne, R. Cornock, C.J. Richards, J. Chung, S. Gambhir, Z. Yue, J. Bourke, B. Zhang, A. Taylor, A. Quigley, R. Kapsa, P. Choong, G.G. Wallace, Development of the Biopen: a handheld device for surgical printing of adipose stem cells at a chondral wound site, Biofabrication (2016), https://doi.org/10.1088/1758-5090/8/1/015019.
[141] C. Di Bella, S. Duchi, C.D. O'Connell, R. Blanchard, C. Augustine, Z. Yue, F. Thompson, C. Richards, S. Beirne, C. Onofrillo, S.H. Bauquier, S.D. Ryan, P. Pivonka, G.G. Wallace, P.F. Choong, In situ handheld three-dimensional bioprinting for cartilage regeneration, J. Tissue Eng. Regen. Med (2018), https://doi.org/10.1002/term.2476.
[142] N. Hakimi, R. Cheng, L. Leng, M. Sotoudehfar, P.Q. Ba, N. Bakhtyar, S. Amini-Nik, M.G. Jeschke, A. Günther, Handheld skin printer:: in situ formation of planar biomaterials and tissues, Lab Chip (2018), https://doi.org/10.1039/c7lc01236e.
[143] U. Tiede, T. Schiemann, K.H. Hoehne, High quality rendering of attributed volume data, in: Proc. IEEE Vis. Conf., 1998, https://doi.org/10.1109/visual.1998.745311.
[144] J.P. Menon, H.B. Voelcker, On the completeness and conversion of ray representations of arbitrary solids, in: Symp. Solid Model. Appl. - Proc., 1995, https://doi.org/10.1145/218013.218057.
[145] Y. Chen, K. Li, X. Qian, Direct geometry processing for telefabrication, J. Comput. Inf. Sci. Eng. (2013), https://doi.org/10.1115/1.4024912.
[146] A. Biswas, V. Shapiro, I. Tsukanov, Heterogeneous material modeling with distance fields, Comput. Aided Geomet. Des. (2004), https://doi.org/10.1016/j.cagd.2003.08.002.
[147] Y. Zhang, T.H. Kwok, An interactive product customization framework for freeform shapes, Rapid Prototyp. J. (2017), https://doi.org/10.1108/RPJ-08-2016-0129.
[148] Y. Zhang, T.H. Kwok, Customization and topology optimization of compression casts/braces on two-manifold surfaces, CAD Comput. Aided Des. (2019), https://doi.org/10.1016/j.cad.2019.02.005.
[149] S. Gerdes, A. Mostafavi, S. Ramesh, A. Memic, I. V Rivero, P. Rao, A. Tamayol, Process–structure–quality relationships of three-dimensional printed poly(caprolactone)-hydroxyapatite scaffolds, Tissue Eng. 26 (2020) 279–291, https://doi.org/10.1089/ten.tea.2019.0237.